

UNCLASSIFIED

AD NUMBER

AD485303

LIMITATION CHANGES

TO:

Approved for public release; distribution is unlimited.

FROM:

Distribution authorized to U.S. Gov't. agencies and their contractors; Critical Technology; MAY 1966. Other requests shall be referred to Air Force Flight Dynamics Laboratory, Attn: FDFR, Wright-Patterson AFB, OH. This document contains export-controlled technical data.

AUTHORITY

AFFDL ltr, 31 May 1973

THIS PAGE IS UNCLASSIFIED

The following notice applies to any unclassified (including originally classified and now declassified) technical reports released to "qualified U.S. contractors" under the provisions of DoD Directive 5230.25, Withholding of Unclassified Technical Data From Public Disclosure.

NOTICE TO ACCOMPANY THE DISSEMINATION OF EXPORT-CONTROLLED TECHNICAL DATA

- 1. Export of information contained herein, which includes, in some circumstances, release to foreign nationals within the United States, without first obtaining approval or license from the Department of State for items controlled by the International Traffic in Arms Regulations (ITAR), or the Department of Commerce for items controlled by the Export Administration Regulations (EAR), may constitute a violation of law.**
- 2. Under 22 U.S.C. 2778 the penalty for unlawful export of items or information controlled under the ITAR is up to ten years imprisonment, or a fine of \$1,000,000, or both. Under 50 U.S.C., Appendix 2410, the penalty for unlawful export of items or information controlled under the EAR is a fine of up to \$1,000,000, or five times the value of the exports, whichever is greater; or for an individual, imprisonment of up to 10 years, or a fine of up to \$250,000, or both.**
- 3. In accordance with your certification that establishes you as a "qualified U.S. Contractor", unauthorized dissemination of this information is prohibited and may result in disqualification as a qualified U.S. contractor, and may be considered in determining your eligibility for future contracts with the Department of Defense.**
- 4. The U.S. Government assumes no liability for direct patent infringement, or contributory patent infringement or misuse of technical data.**
- 5. The U.S. Government does not warrant the adequacy, accuracy, currency, or completeness of the technical data.**
- 6. The U.S. Government assumes no liability for loss, damage, or injury resulting from manufacture or use for any purpose of any product, article, system, or material involving reliance upon any or all technical data furnished in response to the request for technical data.**
- 7. If the technical data furnished by the Government will be used for commercial manufacturing or other profit potential, a license for such use may be necessary. Any payments made in support of the request for data do not include or involve any license rights.**
- 8. A copy of this notice shall be provided with any partial or complete reproduction of these data that are provided to qualified U.S. contractors.**

DESTRUCTION NOTICE

For classified documents, follow the procedure in DoD 5220.22-M, National Industrial Security Program, Operating Manual, Chapter 5, Section 7, or DoD 5200.1-R, Information Security Program Regulation, Chapter 6, Section 7. For unclassified, limited documents, destroy by any method that will prevent disclosure of contents or reconstruction of the document.

485303

AN EXPERIMENTAL STUDY OF THE DISTRIBUTION OF CONVECTIVE HEAT TRANSFER TO A LARGE-SCALE MODEL OF PARACHUTE CLOTH

**E. R. G. ECKERT
J. E. ANDERSON
M. RUIZ-URBIETA
C. J. SCOTT
K. M. KRALL**

UNIVERSITY OF MINNESOTA

TECHNICAL REPORT No. AFFDL-TR-66-13

MAY 1966

This document is subject to special export controls and each transmittal to foreign governments or foreign nationals may be made only with prior approval of the Air Force Flight Dynamics Laboratory (FDFR), W-PAFB, Ohio.

**AIR FORCE FLIGHT DYNAMICS LABORATORY
RESEARCH AND TECHNOLOGY DIVISION
AIR FORCE SYSTEMS COMMAND
WRIGHT-PATTERSON AIR FORCE BASE, OHIO**

485303

NOTICES

When Government drawings, specifications, or other data are used for any purpose other than in connection with a definitely related Government procurement operation, the United States Government thereby incurs no responsibility nor any obligation whatsoever; and the fact that the Government may have formulated, furnished, or in any way supplied the said drawings, specifications, or other data, is not to be regarded by implication or otherwise as in any manner licensing the holder or any other person or corporation, or conveying any rights or permission to manufacture, use, or sell any patented invention that may in any way be related thereto.

Copies of this report should not be returned to the Research and Technology Division unless return is required by security considerations, contractual obligations, or notice on a specific document.

AN EXPERIMENTAL STUDY OF THE DISTRIBUTION OF CONVECTIVE HEAT TRANSFER TO A LARGE-SCALE MODEL OF PARACHUTE CLOTH

**E. R. G. ECKERT
J. E. ANDERSON
M. RUIZ-URBIETA
C. J. SCOTT
K. M. KRALL**

This document is subject to special export controls and each transmittal to foreign governments or foreign nationals may be made only with prior approval of the Air Force Flight Dynamics Laboratory (FDFR), W-PAFB, Ohio.

FOREWORD

This report summarizes the work done by the Heat Transfer Laboratory, Department of Mechanical Engineering, University of Minnesota, during a research program sponsored by the Recovery and Crew Station Branch of the Air Force Flight Dynamics Laboratory under Contract AF33(657)-11688, Project No. 6065, Task No. 606505. The manuscript was released by the authors in January 1966 for publication as an AFFDL Technical Report. The contract's technical project monitor was C. A. Babish III of the Air Force Flight Dynamics Laboratory. E. R. G. Eckert served as principal investigator of the contract at the University of Minnesota.

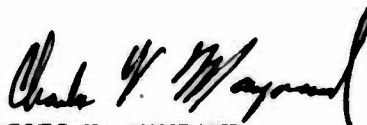
The authors wish to thank other persons on the staff of the University of Minnesota who have contributed to various phases of work. W. Pennel and D. Wilson for their precise work during the acquisition of data and J. Spons for the quality work in the instrumentation of the test model.

The report covers work conducted from December 1964 through December 1965.

This report was submitted by the authors in January 1966.

Information in this report is embargoed under the Department of State International Traffic In Arms Regulations. This report may be released to foreign governments by departments or agencies of the U. S. Government subject to approval of Air Force Flight Dynamics Laboratory (FDFR), or higher authority within the Department of the Air Force. Private individuals or firms require a Department of State export license.

This technical report has been reviewed and is approved.



CHARLES V. MAYRAND
Actg. Chief, Recovery and Crew Station Branch
Air Force Flight Dynamics Laboratory

ABSTRACT

Experiments on pressure distribution and heat transfer on a grid simulating a parachute cloth were performed. The porosity of the grid was 25%. A pressurized wind-tunnel served as the flow facility. The average approach of the flow was 134 feet per second. The pressure ratio P_{up}/P_{down} was considered as the main variable and varied from around 11 to 1.45. A transient energy balance was used to calculate local heat transfer.

CONTENTS

SECTION	PAGE
I. INTRODUCTION	1
II. EXPERIMENTAL EQUIPMENT	4
A. Facility	4
B. Heating Chamber	4
C. Instrumentation	5
1. Pressure	5
2. Temperature	5
D. The Experimental Model	6
III. EXPERIMENTAL STUDIES	9
A. Uniformity of Approach Flow	9
B. Surface Pressure Distribution	9
C. Recovery-Temperature Runs	10
D. Heat Transfer Runs	13
IV. CONCLUSIONS	16
REFERENCES	17
APPENDIX - Transient Energy Balance	49

ILLUSTRATIONS

FIGURE		PAGE
1	Heating apparatus, pneumatic piston, steel windows for Schlieren pictures.	18
2	Heating chamber, with the test model.	19
3	Typical photograph of the manometer board used to read the pressure distribution.	20
4	View of the test model; (a) without supporting pieces, and (b) with supporting pieces.	21
5	Detailed sketch of the test model.	22
6	Cross-sections where measurements were taken.	23
7	Typical instrumentation of two cross-sections corresponding to Bars 2 and 1, respectively.	23
8	Sketch of the test section of the wind tunnel.	24
9	Pressure distribution for Cross-Section A-A.	25
10	Pressure distribution for Cross-Section B-B.	26
11	Pressure distribution for Cross-Section C-C.	27
12	Pressure distribution for Cross-Section A'-A'.	28
13	Pressure distribution for Cross-Section B'-B'.	29
14	Pressure distribution for Cross-Section C'-C'.	30
15	Recovery temperature distribution for Cross-Section A-A.	31
16	Recovery temperature distribution for Cross-Section B-B.	32

ILLUSTRATIONS (cont'd)

FIGURE		PAGE
17	Recovery temperature distribution for Cross-Section C-C.	33
18	Recovery temperature distribution for Cross-Section A'-A'.	34
19	Recovery temperature distribution for Cross-Section B'-B'.	35
20	Recovery temperature distribution for Cross-Section C'-C'.	36
21	Distribution of the heat transfer coefficients for Cross-Section A-A.	37
22	Distribution of the heat transfer coefficients for Cross-Section B-B.	38
23	Distribution of the heat transfer coefficients for Cross-Section C-C.	39
24	Distribution of the heat transfer coefficients for Cross-Section A'-A'.	40
25	Distribution of the heat transfer coefficients for Cross-Section B'-B'.	41
26	Distribution of the heat transfer coefficients for Cross-Section C'-C'.	42
27	Distribution of the heat transfer coefficients in polar form for Cross-Section A-A.	43
28	Distribution of the heat transfer coefficients in polar form for Cross-Section B-B.	44
29	Distribution of the heat transfer coefficients in polar form for Cross-Section C-C.	45
30	Distribution of the heat transfer coefficients in polar form for Cross-Section A'-A'.	46
31	Distribution of the heat transfer coefficients in polar form for Cross-Section B'-B'.	47
32	Distribution of the heat transfer coefficients in polar form for Cross-Section C'-C'.	48

ILLUSTRATIONS (cont'd)

FIGURE		PAGE
33	Typical extrapolation technique for heat transfer coefficient.	56
34	Typical temperature-time history.	57

NOMENCLATURE*

A	convective heat transfer area, ft. ²
a	speed of sound, ft. /sec.
C_p	specific heat, Btu/lb. °F.
D	outside diameter of the bar, ft.
h	convective heat transfer coefficient, Btu/hr.ft. ² °F.
k	thermal conductivity, Btu/hr.ft. °F.
p	absolute static pressure, inches of Hg.
q	rate of heat transfer per unit area, Btu/hr. -ft. ²
R	dimensionless temperature ratio
r	ratio adiabatic wall temperature to stagnation temperature
T	temperature, °R
t	thickness, ft.
ε	radiations' interchange factor
θ	angle measured around the model from upstream direction
μ	viscosity, lb. /sec. ft.
ρ	density, lb _m /ft ³
σ	Stephan-Boltzmann constant, Btu/ft. ² hr. °R ²
τ	time, hr.

*Several symbols defined in the text and used but briefly, are not included in this list.

NOMENCLATURE (cont'd)

Superscripts

- * denotes same condition calculated from the stagnation conditions upstream, assuming an isentropic expansion to sonic velocity

Subscripts

- aver. average value
- aw denotes adiabatic wall condition
- down denotes conditions downstream
- m refers to model material
- o denotes stagnation conditions in main stream
- stag denotes conditions at the stagnation point
- up denotes conditions upstream
- w denotes local conditions at the model surface

I. INTRODUCTION

This report describes the methods and results of an experimental program to determine the convective heat transfer to the cloth of a parachute designed to decelerate vehicles from supersonic speeds. Since instrumentation difficulties precluded the possibility of determining the distribution of heat flux to the fiber of which the cloth is composed, the experimental program was divided into two parts; the microscale study and the macroscale study. In the microscale study, reported in this document, an enlarged model of the woven fiber was built and instrumented to determine how the heat flux is distributed to the fiber. In this model, the simulated fibers were one inch in diameter. In the macroscale study, to be reported later, the gross convective heat transfer per unit area to an actual scale model of the woven cloth was determined. The porosity of the microscale-study grid was fixed by mass flow considerations for existing tunnel facilities. The incoming feed lines along with the quick opening valve fixed the incoming mass flow. Then the model porosity was computed to produce a sonic throat in and at the open area minimums. On this basis, the grid was built with a porosity of 25%. The macroscale-study grid duplicates the actual size and porosity of a representative parachute mesh cloth.

The experimental facility used in the microscale study is located at the University of Minnesota's Rosemount Research Center. It was used before to obtain corresponding results reported in Reference 1 on a model of a ribbon parachute. For the present microscale study, two differences in procedure from those used in Reference 1 were made. The first involves the operating pressure level. In Reference 1 the air entered the wind tunnel from a compressor, where it was dried to a dew point of -40°F , and was exhausted into the atmosphere. In the present study, however, due to the fact that the model is larger than full scale the sonic Reynolds number is increased proportionally. The sonic Reynolds number may be defined as

$$Re^* = \frac{\rho^* a^* D}{\mu^*}$$

Since the heat transfer depends on the Reynolds number, essentially constant throughout this study, it was desirable to compensate for this increase by reducing the pressure and hence the density of the flow. For this reason, it was decided to take air directly from the atmosphere and exhaust it into a vacuum tank. With this change, the Reynolds number was between 700,000 and 900,000. Unfortunately, in doing this it was inconvenient to dry the incoming air. In the first experimental runs made to determine the heating rate of the model, the necessary difference between the initial model temperature and the steady state (recovery) temperature was

obtained in the same way as in Reference 1. In this method the model was cooled with dry snow (CO_2) to a temperature of about -110°F before inserting it into the wind tunnel; however, in the present experiments the moisture in the undried air was often seen to produce a frost layer on the model. Since this frost layer would influence the results by an unknown amount, it was decided to revise the procedure (the second difference from Reference 1) by heating the model prior to insertion into the wind tunnel. This procedure was actually found to be quicker and still provided a sufficiently uniform initial temperature.

In the following sections, the important pieces of special equipment used in the tests and the model itself are described first. Following this, measurements of the pressure distribution around the model are discussed. Then the two main parts of the experimental program are described separately. First are the recovery-temperature measurements needed to find the steady-state temperature of the model in the flowing stream, and second are the transient temperature measurements needed to find the heating rate. The details of the procedure used to compute the heat transfer coefficients from the data of the two types of measurements are given in the Appendix. Data were taken at six different pressure ratios. These varied from eleven, which was the highest obtainable with the facility used, to 1.45, which was as close to unity as was felt to be of interest.

II. EXPERIMENTAL EQUIPMENT

A. Facility

The experimental facility used is the same as described in Section IIA of Reference 1, and shown in Figure 2 of that reference with the following exceptions:

1. Upstream of the test section the air was taken directly from the atmosphere and therefore the compressed air system was not used.
2. Downstream of the model air was led into the vacuum tanks. The vacuum system has a capacity of 22,750 cubic feet and is evacuated by two Allis-Chalmers 27-D vacuum pumps. These pumps, rated at 3390 cfm each, are powered by a 350 h. p. motor, which drives both pumps. The lowest vacuum obtainable with the pumps in series was 2" Hg.

B. Heating Chamber

To carry out the heat transfer measurements it was necessary to heat the model to a constant temperature before inserting it into the air stream. Figures 1 and 2 show two different views of the apparatus constructed to do this. The pneumatic piston in these figures made possible the insertion and removal of the model as fast as necessary. By regulating the valves it was possible to avoid destructive impacts against the wind-tunnel windows. The chamber exterior was built with removable

top and bottom plates to facilitate handling of the heater. The heater consists of coiled Nichrome wire uniformly distributed on two removable asbestos plates placed on the side walls of the heating chamber. During the heating period the top plate was kept closed. The Dymec system described in Subsection C, monitored the temperature distribution during this period.

C. Instrumentation

1. Pressure

In order to measure the pressure distribution the mercury manometer board shown in Figure 2 of Reference 1 was used. Pressure differences could be read with an uncertainty of ± 0.025 inches of mercury. A quick acting valve at the top clamped the leads from the model, thus holding the reduced pressure. At this moment readings were taken by photographing the manometer board so that the readings could be rechecked. One of these photographs is shown in Figure 3. The pressure taps were silver-soldered in holes 0.028 inches in diameter and drilled in the wall. Figure 7 gives a detailed explanation. The outside surface was repolished after this installation. All pressure taps were tested and found to be leakproof.

2. Temperature

Thirty gauge, roll calibrated iron-constantan thermocouples were inserted approximately $1/32$ inch in the wall of the model.

After this the thermocouples were silver-soldered.

Modification M24 of the Dymec DY-2010A Data acqisitor's system provided 25 channel inputs continuously monitored at a precise rate of 5 channels a second, with digital read out.

D. The Experimental Model

Two general views of the test model or grid are shown in Figure 4. It consists of seven highly polished bars of free machining stainless steel, arranged in such a way that they resemble woven cloth of 25% porosity. Stainless steel was chosen because of its relatively small thermal conductivity and corrosion resistance. It should be recalled, however, that since only the rate of heat transfer through the air to the surface is being considered, the material used in the model can be chosen at the discretion of the experimenter.

Bars 1, 2, and 3, Figure 5, are hollow with 1/16" wall thickness. Bar 1 contains the pressure taps and Bar 2 the thermocouples. Because of the influence of the thickness of these hollow bars in the calculation of the heat transfer coefficients, the bars were made as accurate as possible within a tolerance of $\pm .003$ inches. Bar 3 was also made hollow because it is in contact with Bars 1 and 2, and the rest of the bars are solid. Bars 1, 2, and 3 were assembled by cementing together two parts which were mirror images.

The model is held together by two thin plates, one at the top and one at the bottom (see Figure 4b), and two heavier pieces which fit snugly into steel "windows" in the two opposite wind-tunnel walls as shown in Figure 1. With this construction, it was possible to retract the model from the wind-tunnel to heat it up to the desired temperature. The optical windows shown on Figure 1 are provided for shadowgraph/schlieren observations of the flow.

With respect to the orientation of the model with the direction of flow, measurements were taken at the six circular cross sections indicated in Figure 6. The necessary information was obtained from five of these cross sections while the sixth, C-C or C'-C', served to check the symmetry of the flow. This symmetry is more apparent from Figure 5 which shows the proximity of the instrumented bar with respect to all neighboring perpendicular bars. As mentioned above, however, Bar 1 was instrumented only with pressure taps and Bar 2 only with thermocouples. Readings at all six cross sections shown in Figure 6 were therefore obtained by rotating the model 180° and repeating the run. Thus cross sections A-A, B-B, and C-C are transformed into cross sections A'-A', B'-B', and C'-C', respectively by turning the model around.

The symmetry of the flow with respect to the horizontal axes X-X and Y-Y, respectively, shown in Figure 7, made it necessary to place instrumentation around only half of the cross sections. The half cross

sections instrumented were those farthest from the wind-tunnel walls.

The cross sections are instrumented at seven peripheral locations corresponding to the angles $\theta = 0^\circ, 30^\circ, 60^\circ, 90^\circ, 120^\circ, 150^\circ$, and 180° measured from the upstream side with the exception that in cross sections A-A and A'-A' there is no instrumentation at the point of contact. See Figure 7.

III. EXPERIMENTAL STUDIES

A. Uniformity of Approach Flow

According to the measurements taken in the summer of 1964 by Eckert and Scott on the same wind tunnel, the upstream velocity distribution is as given in Figure 8 of Reference 1. All velocities are within 1% of the centerline velocity with the exception of the four points taken near the nozzle walls.

B. Surface Pressure Distribution

The pressure distribution around the model in the cross-sections A-A, B-B, and C-C was measured at different pressure ratios P_{up}/P_{down} . The model was then turned 180° around a horizontal axis through its mid-point, as explained in Section IID, and the runs were repeated. In this case, the pressure distribution was measured at the cross sections A'-A', B'-B', and C'-C'.

Since the air was taken directly from the atmosphere through a piping system, the total pressure P_{up} varied only with the atmospheric conditions. One wall static pressure tap located upstream, (see Figure 8), where the velocity of the air is negligible, gave $P_{up} \approx P_{stag}$. Another wall static pressure tap located in the centerline of the last window (see Figure 8), was used to measure P_{down} .

Figures 9 through 14 show the ratio P/P_{up} as a function of the angle θ , for the six cross-sections. The almost constant pressure distribution around the cross-section A-A, Figure 9, can be explained by the fact that the flow is retarded by the presence of the rearward bar, thus causing the pressure to remain near the stagnation pressure. The rest of the figures show that the pressure distribution around the upstream portion of the cross-section is independent of pressure ratio up to a certain value of the angle θ , say θ_g . This can be explained on the basis of Schlichting's theory of separation (Reference 2). This theory states that the angle θ at which separation occurs increases with pressure ratio, P_{up}/P_{down} . Thus we can infer that the point θ_g , at which the pressure distribution curve for a given pressure ratio breaks away from the curves for higher pressure ratios, is the separation point.

Some differences in the pressure distributions given by Figures 11 and 14, which correspond to cross-sections having the same orientation with respect to the flow are probably due to the non-perfect symmetry of the flow and to the non-perfect alignment of the model bars.

C. Recovery Temperature Runs

To calculate the heat transfer coefficients by the method described in the Appendix, the recovery temperature, also called adiabatic wall temperature, must be known. The recovery temperature at each point around a surface is the temperature that this point assumes

in steady state under the influence of internal friction in the boundary layer where the convective heat flux has the value zero.

At the highest pressure ratio, $P_{up}/P_{down} \approx 11-12$, the characteristic running time of the wind tunnel was about 4 minutes. After this time it was not possible to maintain a constant pressure ratio since the pumping system was not able to pump out the air flowing into the vacuum tanks. Because of this the downstream pressure started to increase and the pressure ratio decreased. The rate of change of the pressure ratio decreased with decreasing pressure ratio.

Data on recovery temperatures were taken at five different pressure ratios. These data give sufficient information because of the small changes of the recovery temperature with the pressure ratio as explained below. Two of these pressure ratios are supercritical, two are subcritical and the fifth one close to the critical pressure ratio.

In taking the data at the highest pressure ratio, it could be observed that, after the 4-minute interval, during which the pressure ratio remained constant, the rate of change of the temperature was at all points less than $.02^{\circ}\text{F}/\text{sec}$. Hence the last temperatures measured were taken as the recovery temperatures and no extrapolations were necessary. To obtain the recovery temperature at the lower pressure ratios, the wind tunnel was kept running beyond the 4-minute interval. As the pressure ratio gradually decreased, each set of temperature

readings were taken at different pressure levels symmetrical around each desired pressure ratio; the first one before, the second one at, and the third one after reaching the desired pressure ratio. As all three of these sets of readings showed nearly the same temperatures, these temperatures were taken as the recovery temperatures. This meant essentially that the time constant for temperature relaxation was small compared to the time rate at which the pressure changed. After 20 minutes running time the lowest pressure ratio was reached. By plotting T_{aw}/T_o vs. P_{up}/P_{down} it was found that the points corresponding to the highest and lowest pressure ratio were different by less than 2%. This supported the idea of accepting the temperature measured in the manner indicated as the recovery temperature. A very slight increase of the recovery temperature with decreasing pressure ratio could be observed.

During the recovery temperature runs, data were taken at three different cross sections at the same time. A total of 21 thermocouples were used, 20 of them at the three cross sections and the other one placed upstream to measure the stagnation temperature of the air T_o . This last one had two connections to the Dymec, so that it was possible to get more accurate information about the variations of the air stagnation temperature during the 4.4 seconds required for the Dymec to take the readings.

The temperature variations of the air stagnation temperature have been less than $\pm 0.5^\circ\text{F}$, during each run.

Each run was repeated and showed consistent results. The ratio T_{aw}/T_o of the absolute temperatures has been plotted as functions of the angle θ in Figures 15 through 20. Cross sections A-A, B-B, and C-C indicated higher ratios of T_{aw}/T_o at corresponding angles θ , than cross sections A'-A', B'-B', and C'-C'. Cross sections C-C and C'-C' should show the same results. The difference may be attributable to a probable change of the relative humidity of the air, to the non-perfect symmetry of the flow, and to non-perfect alignment. The figures indicate that the temperature recovery is almost 100% over the upstream part of the model as well as in the separated flow regime.

D. Heat Transfer Runs

In order to get the desired information on the local heat transfer, transient data were also taken in the cross sections mentioned above. The general heat transfer experimental technique is described in detail in the Appendix. As mentioned above, the technique required preheating the model with an electric heater to a temperature significantly different from the recovery temperature. To avoid circumferential heat conduction in the model it was more important to obtain a uniform temperature distribution at the start of each run than to get a prescribed temperature. By observing the temperature readings on the Dymec during the heating period, it was possible to initiate the run when the temperatures were sufficiently uniform. In general the model was heated to around 250°F.

The largest temperature difference in the cross section was always less than 10°F . The conduction error in the heat transfer coefficients produced by this difference was estimated and found negligible. Once the temperature distribution was uniform to this degree, the model was inserted in the wind tunnel in less than $1/2$ second. At the same time two operators opened the upstream quick-opening DC Zurik valve and the Butterfly valve downstream between the wind tunnel and the vacuum tanks. In total, the system was operating in less than 1 second. Owing to the rapid cooling of the grid upon insertion into the tunnel, rapid measurements of wall temperatures were necessary. Thus only one cross-section was studied in each heat transfer run.

The heat transfer coefficients were extrapolated to zero time ignoring data taken in the first second, since this data gave unreliable results arising from disturbances created by the actual insertion of the test grid. The reader is again referred to the Appendix where a sample run and the various steps in the data reduction are illustrated.

Data were taken at six different pressure ratios, three of them corresponding to supercritical pressure ratios, two to subcritical ratios, and the sixth one near the critical pressure ratio.

Local heat transfer coefficients are presented in Figures 21 through 26 in Cartesian coordinates and in Figures 27 to 32 in polar diagrams. The influence of the pressure ratio on heat transfer is somewhat puzzling. This may be due to the complicated geometry and also possibly to the fact that the humidity in the air was rather high on

days at which some of the experiments were run. On the other hand, the pressure distribution curves in Figures 11 through 16 exhibit quite a regular decrease of pressures with increasing pressure ratio and show no indication of a humidity influence. To draw curves for each pressure ratio in the figures would have confused the picture. Therefore only an average curve has been indicated in Figures 21 through 23 and 25. The measured points in Figures 24 and 26 separate clearly into two groups: one for subcritical and the other for supercritical pressure ratio. Two curves have therefore been drawn in these figures.

Figures 27 through 32 repeat the curves contained in the preceding figures in polar diagrams. One or two scales have been added which allow the ratio of local to average heat transfer coefficients to be read. It is felt that this ratio is especially useful in design calculations. The value of the average heat transfer coefficients itself can easily be read from the left-hand scale.

IV. CONCLUSIONS

Experiments have been performed to determine local convective heat transfer to a model simulating the shape of parachute cloth with a porosity of 25%. The pressure ratio P_{up}/P_{down} was varied from subcritical to supercritical values in the range of 1.45 to approximately 11. The upstream total pressure was close to atmospheric.

Pressure distribution, recovery temperatures, and convective heat transfer coefficients have been obtained and are presented in Figures 9 through 32. The complicated nature of the flow prevented any analytical treatment.

REFERENCES

1. C. J. Scott and E. R. G. Eckert, "Experiments on the Thermal Performance of Ribbon Parachutes," AFFDL-TR-64-192, December, 1964.
2. H. Schlichting, "Boundary Layer Theory," McGraw-Hill Book Company, Inc., New York, 1960.

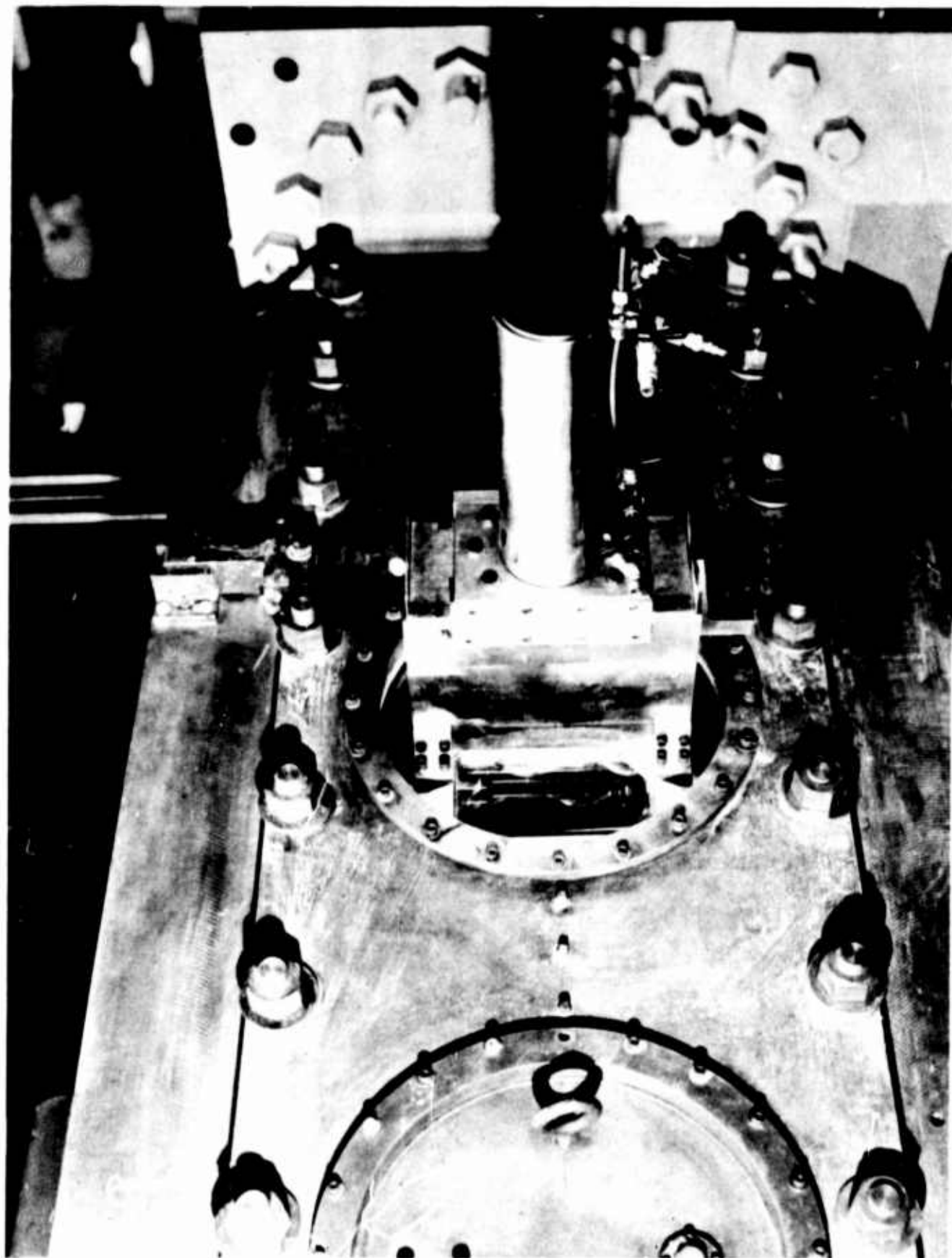


FIGURE 1 HEATING APPARATUS, PNEUMATIC PISTON, STEEL WINDOWS FOR
SCHLIEREN PICTURES

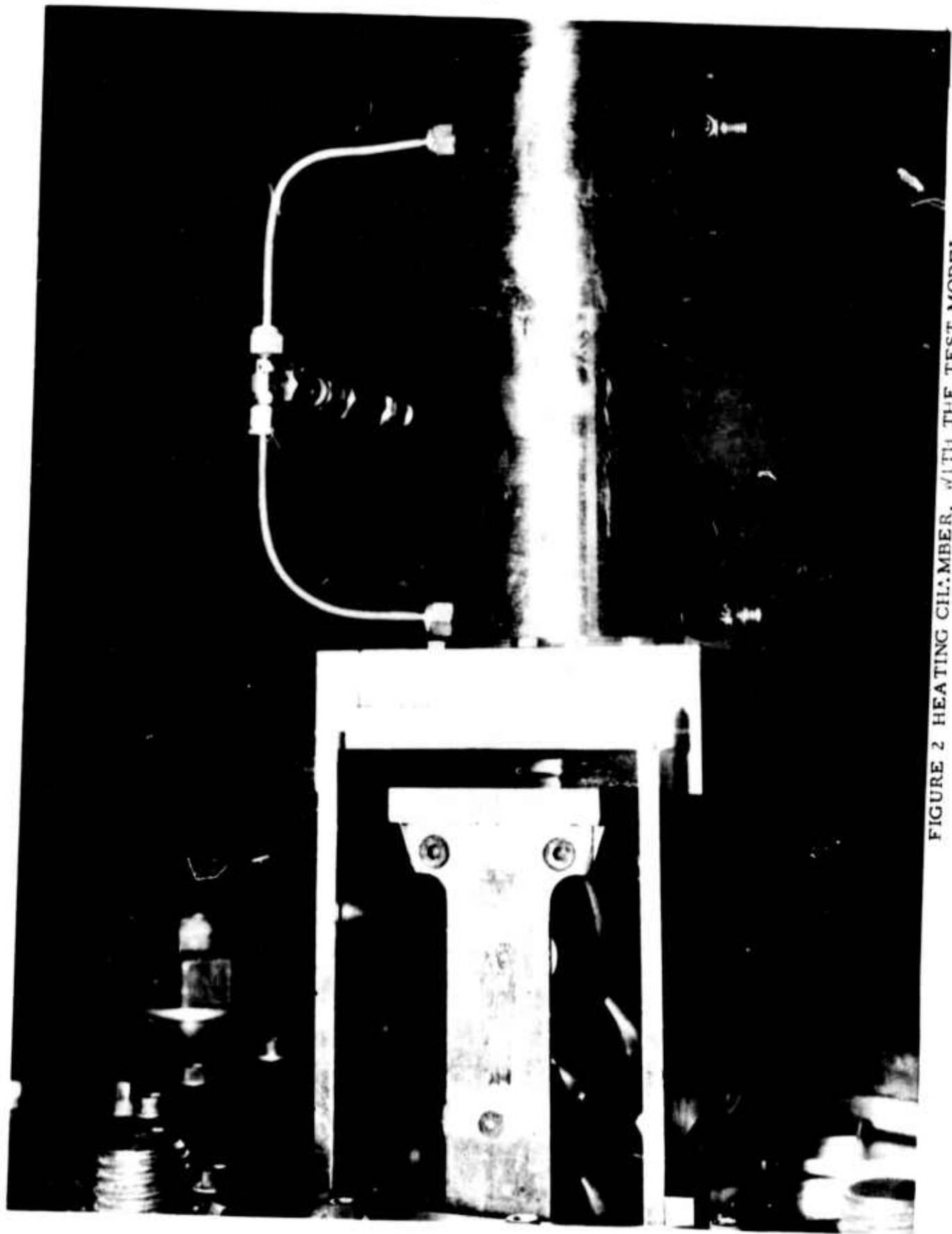


FIGURE 2 HEATING CHAMBER, WITH THE TEST MODEL

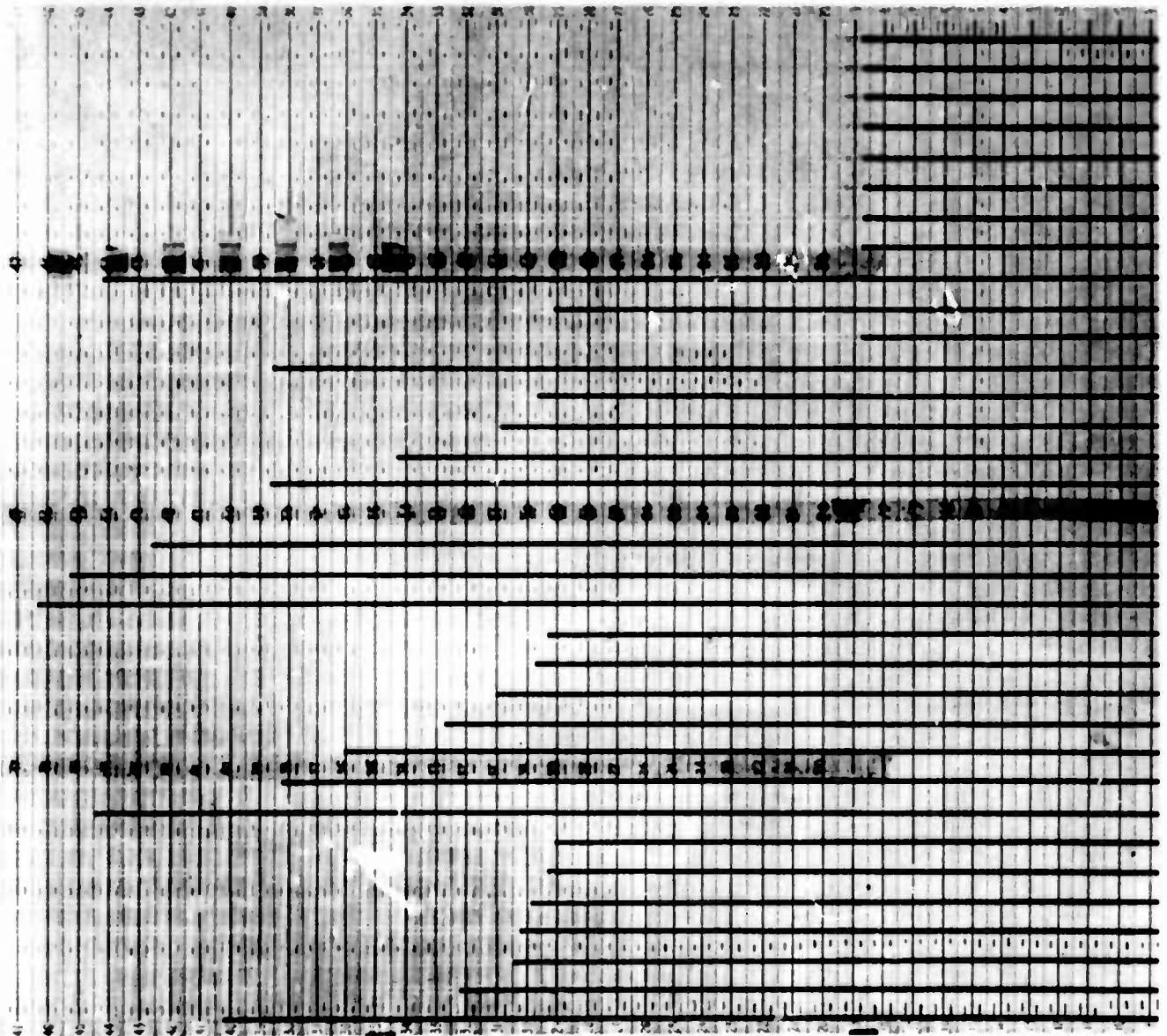


FIGURE 3 TYPICAL PHOTOGRAPH OF THE MANOMETER BOARD USED TO READ THE PRESSURE DISTRIBUTION

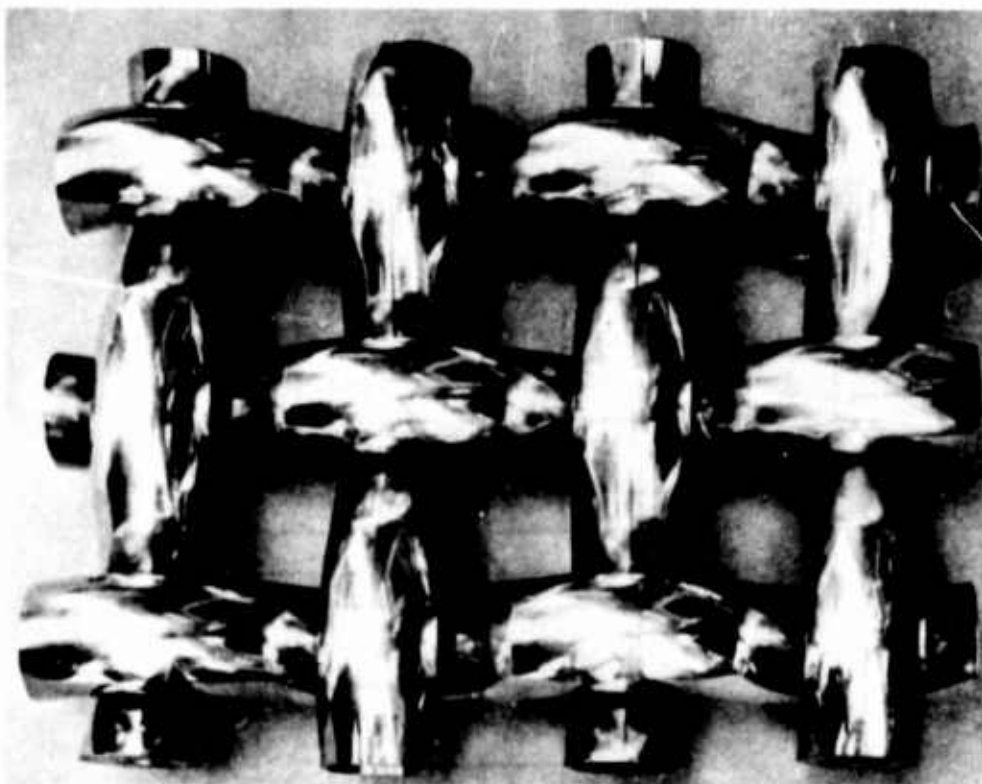


FIGURE 4a VIEW OF THE TEST MODEL WITHOUT SUPPORTING PIECES

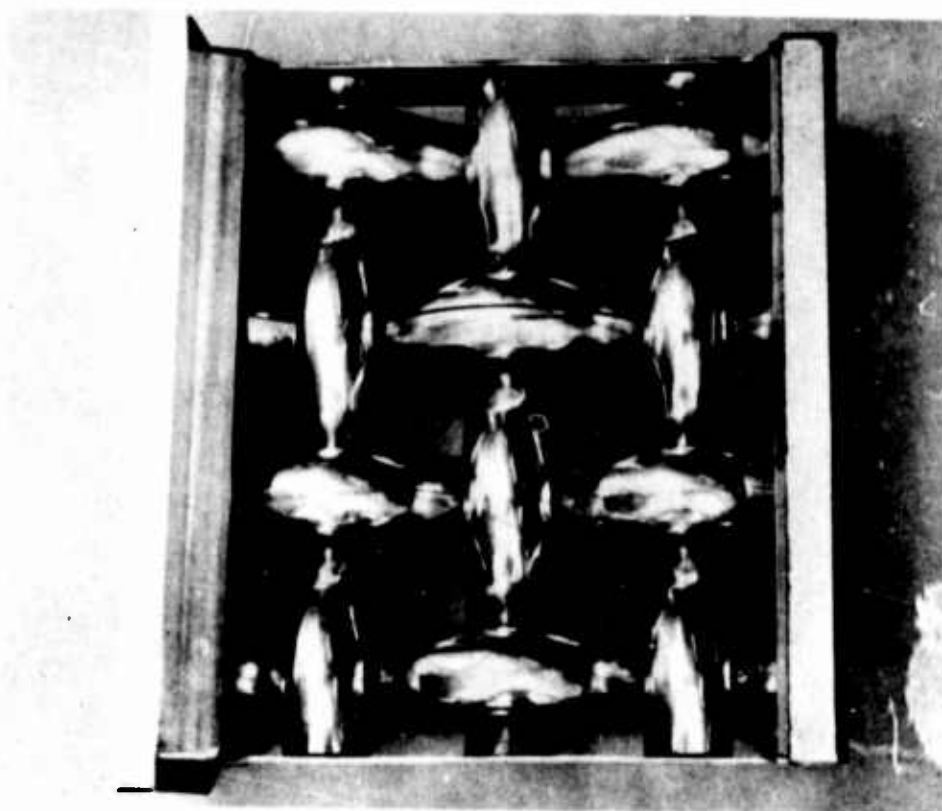
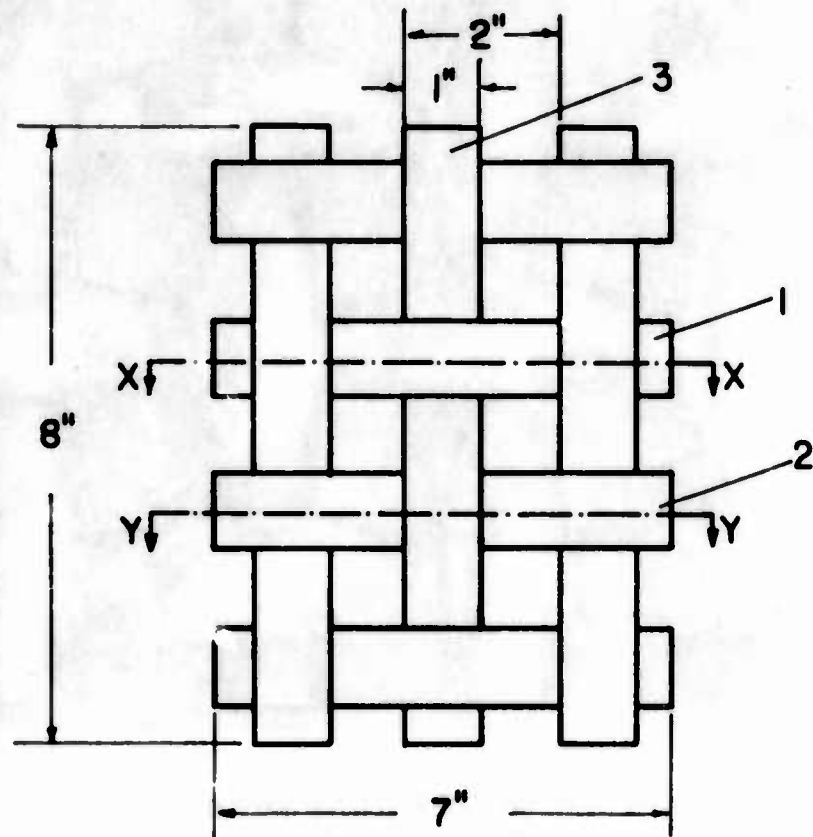
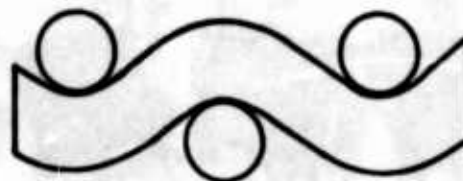


FIGURE 4b VIEW OF THE TEST MODEL WITH SUPPORTING PIECES



Cross-Section Y-Y



Cross-Section X-X

FIGURE 5 DETAILED SKETCH OF THE TEST MODEL.

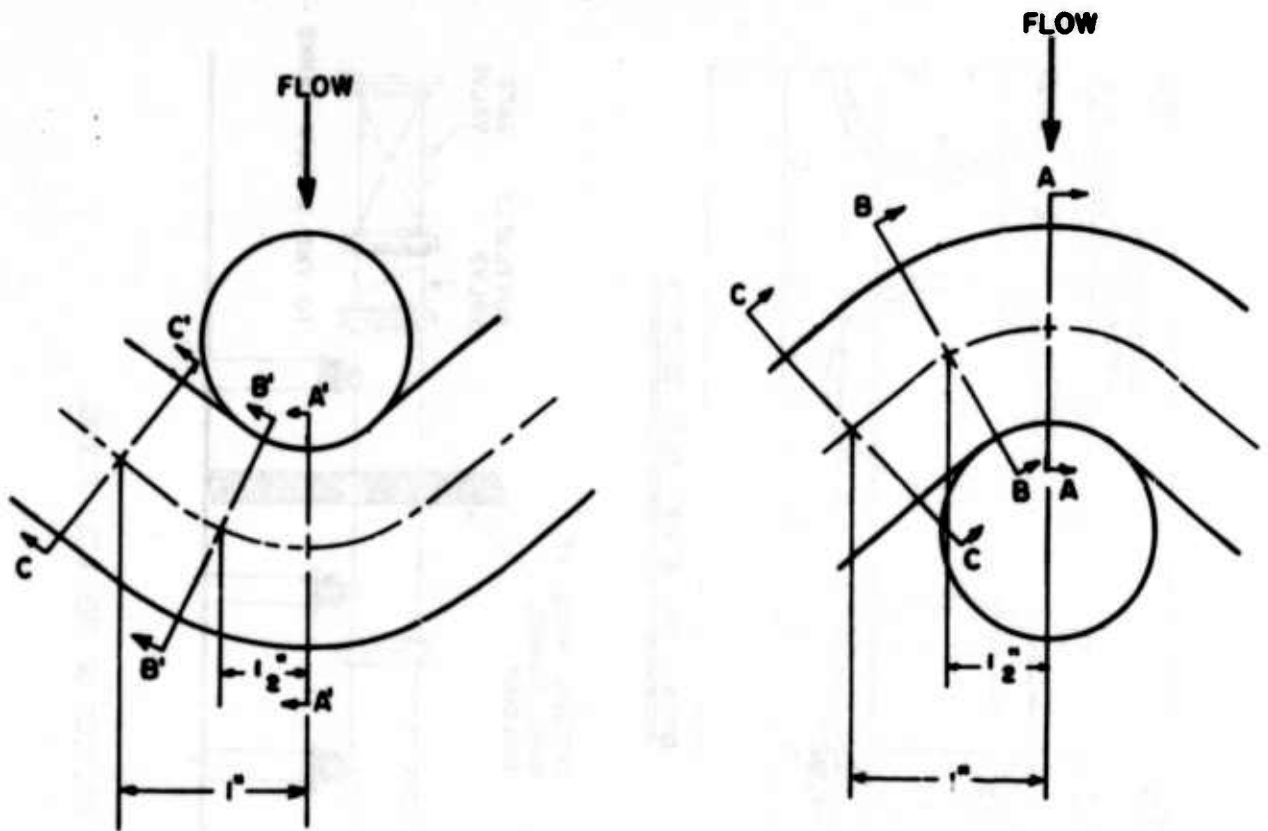


FIGURE 6 CROSS SECTIONS WHERE MEASUREMENTS WERE TAKEN

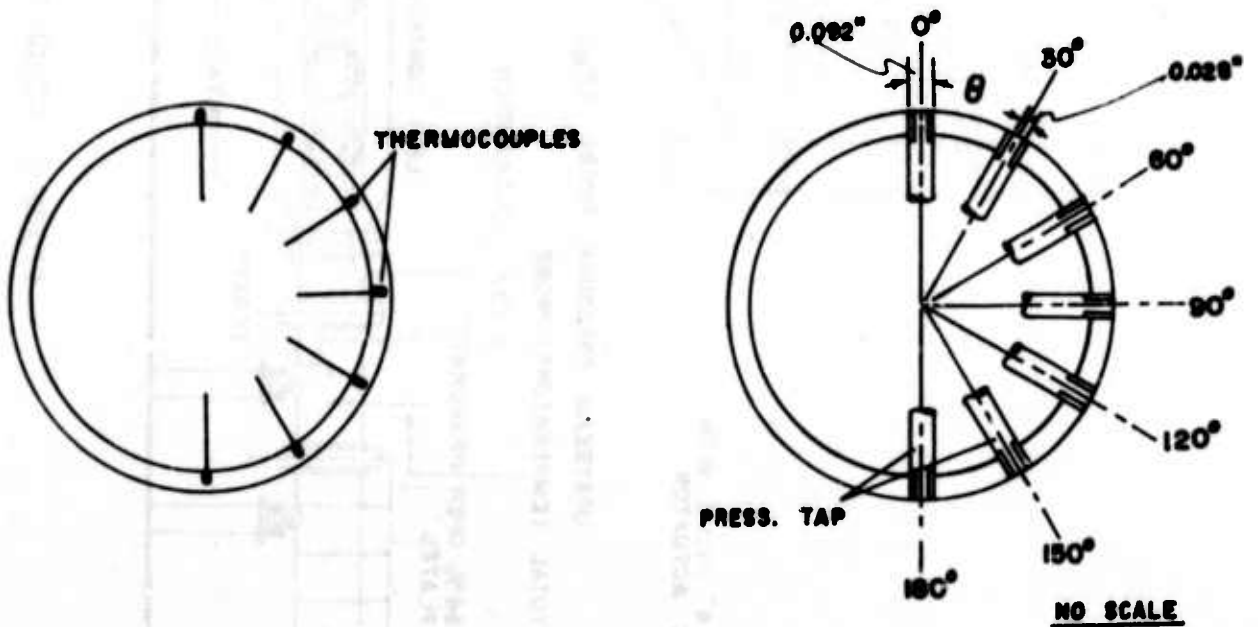


FIGURE 7 TYPICAL INSTRUMENTATION OF TWO CROSS-SECTIONS CORRESPONDING TO BARS 2 AND 1, RESPECTIVELY

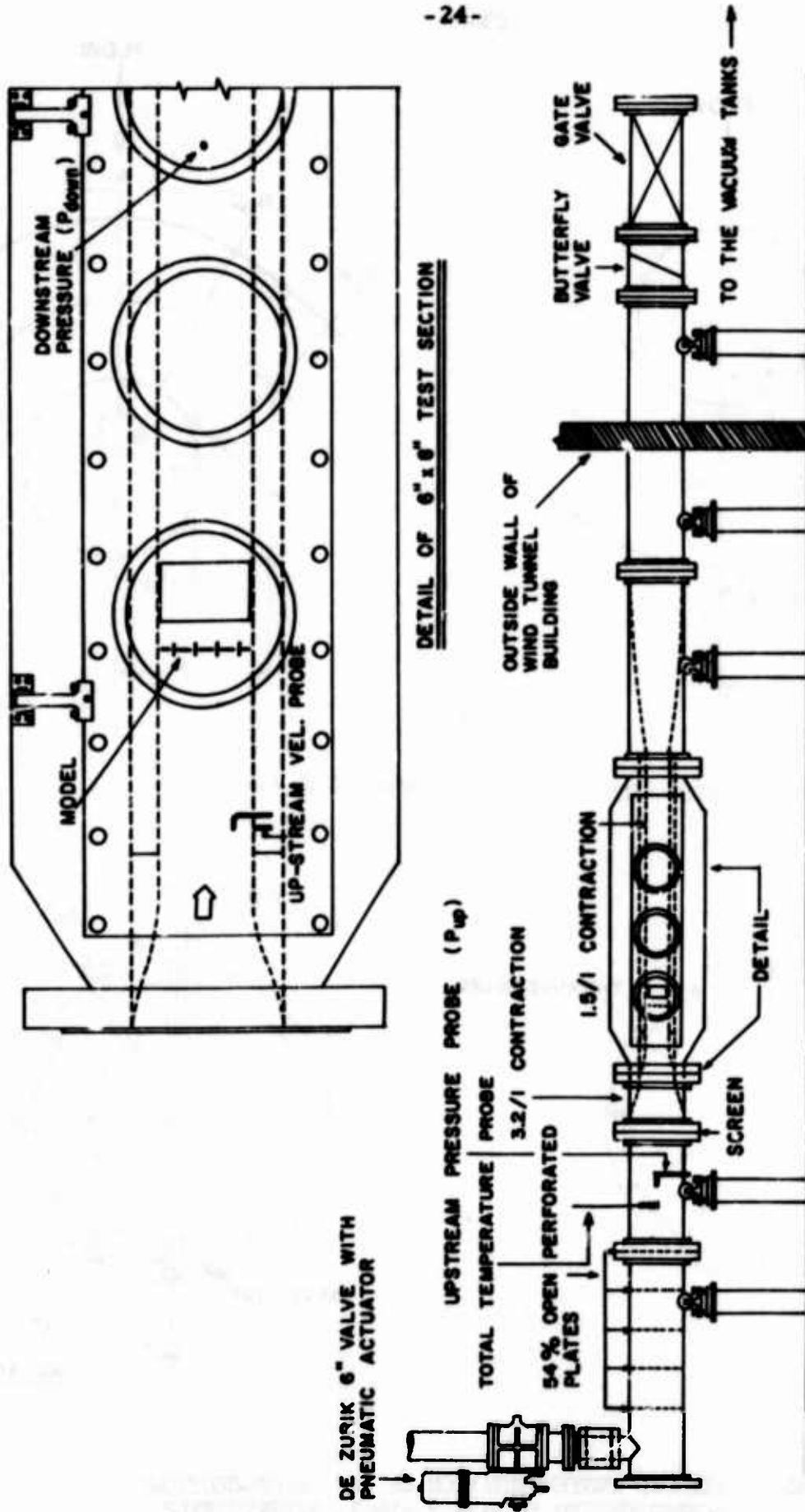


FIGURE 8 SKETCH OF THE TEST SECTION OF THE WIND TUNNEL

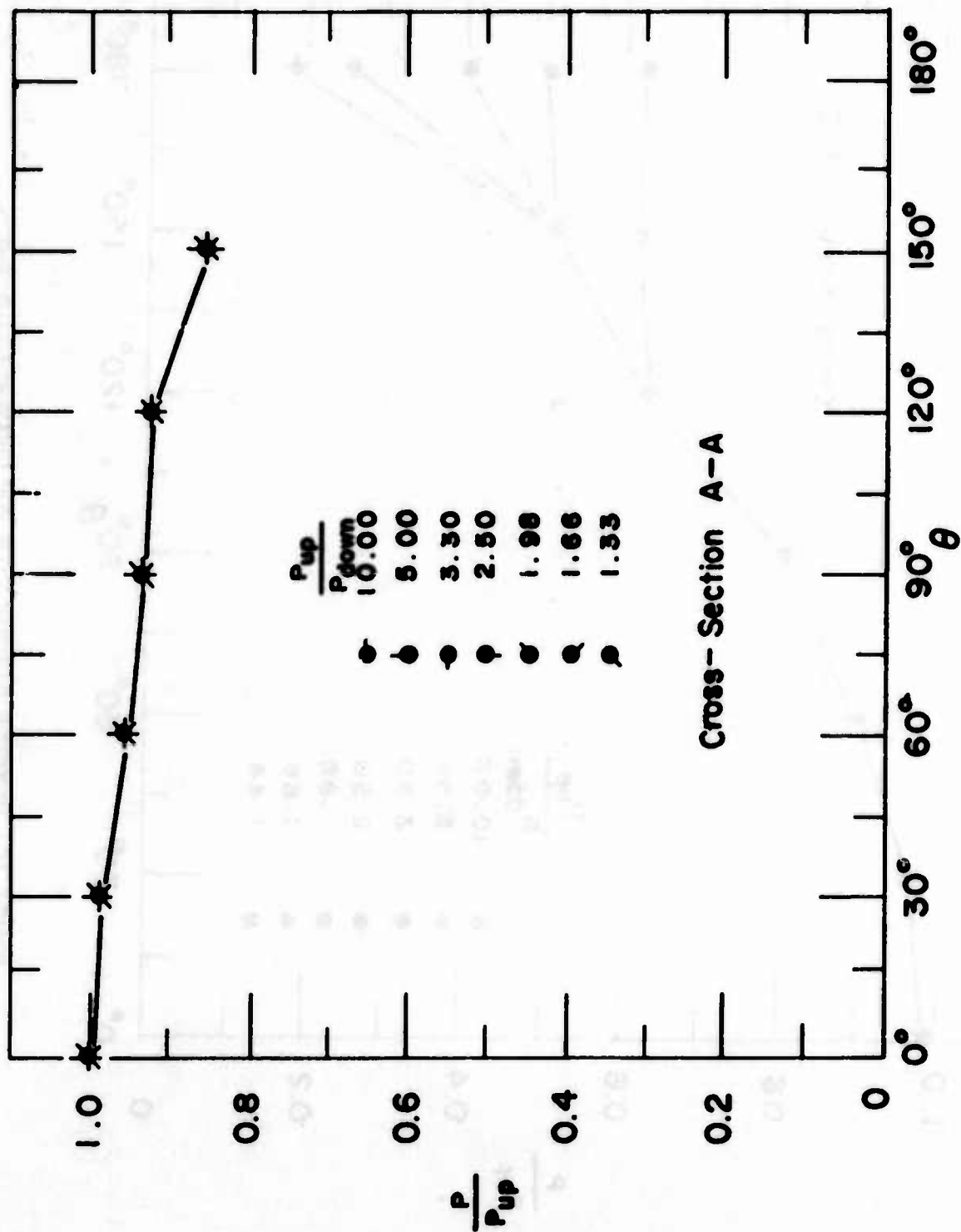


FIGURE 9 PRESSURE DISTRIBUTION FOR CROSS SECTION A-A

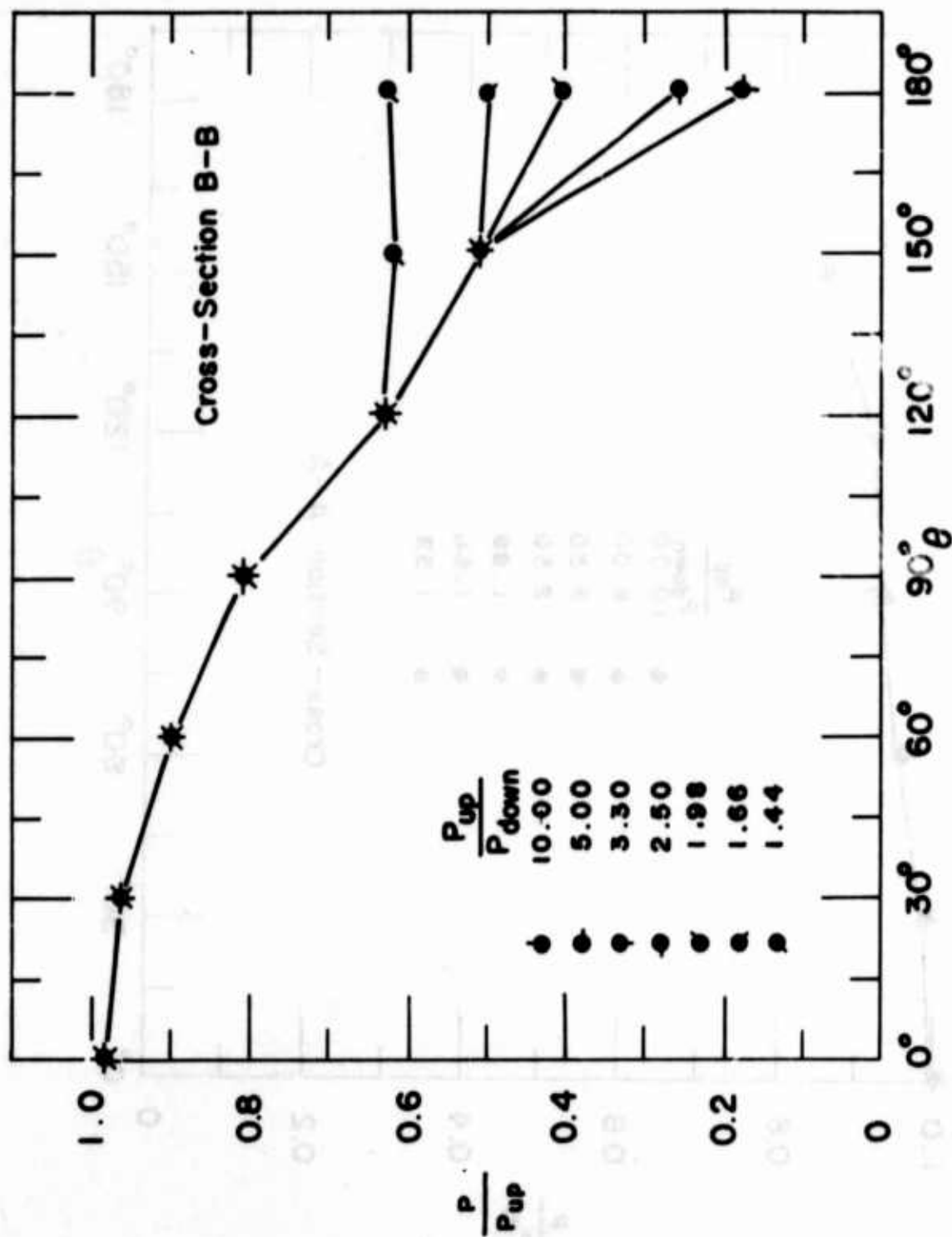


FIGURE 10 PRESSURE DISTRIBUTION FOR CROSS-SECTION B-B

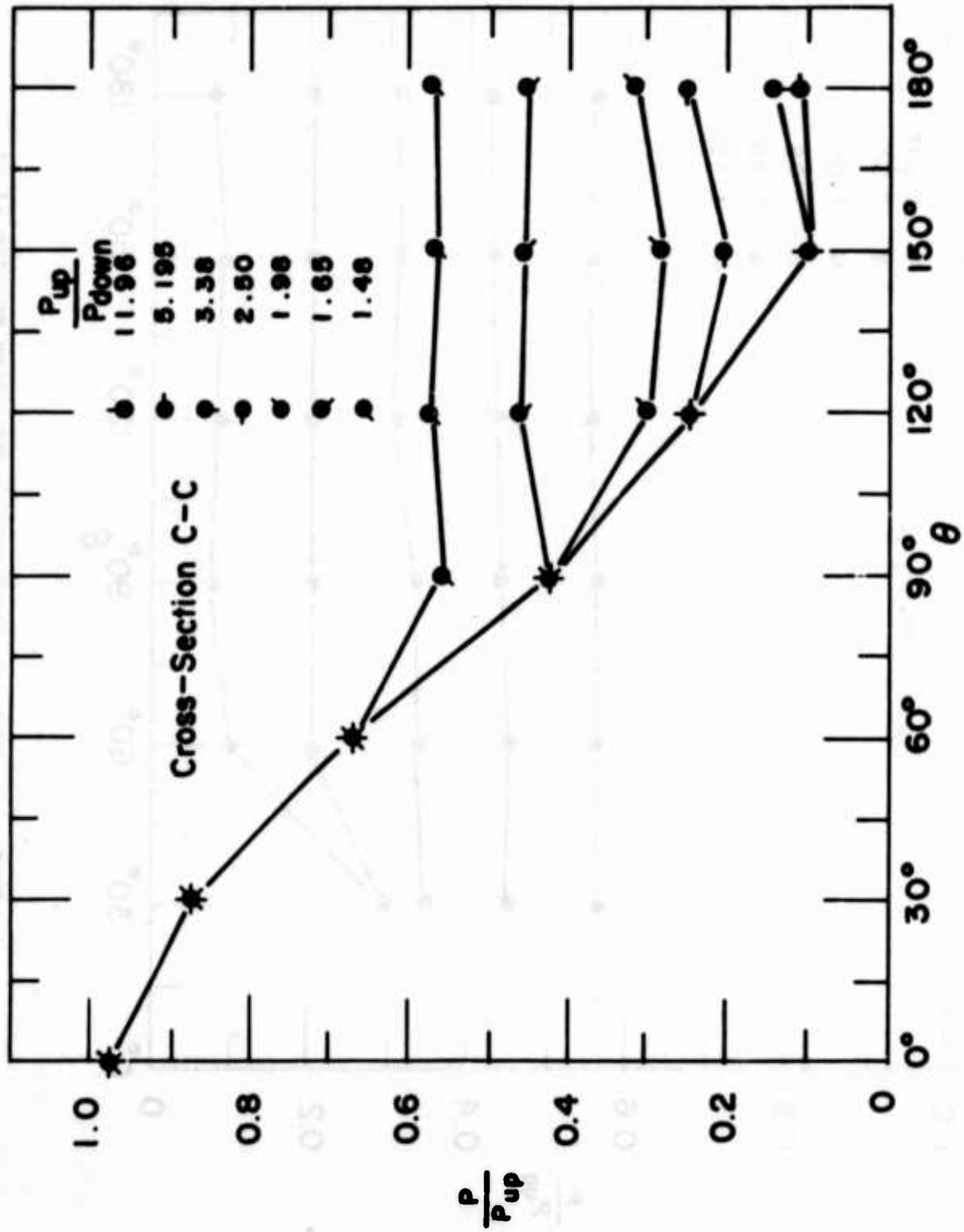


FIGURE 11 PRESSURE DISTRIBUTION FOR CROSS-SECTION C-C

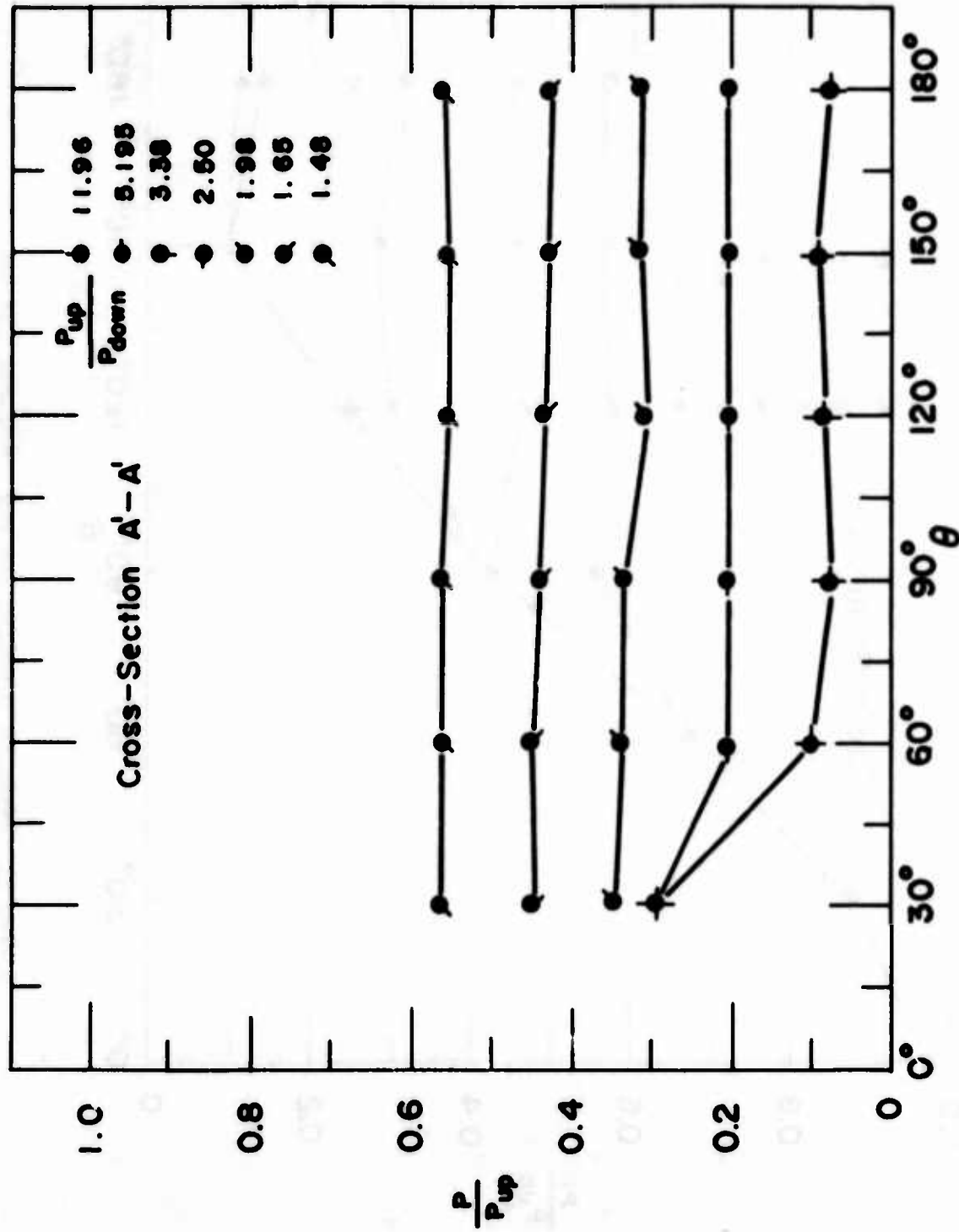


FIGURE 12 PRESSURE DISTRIBUTION FOR CROSS-SECTION A'-A'

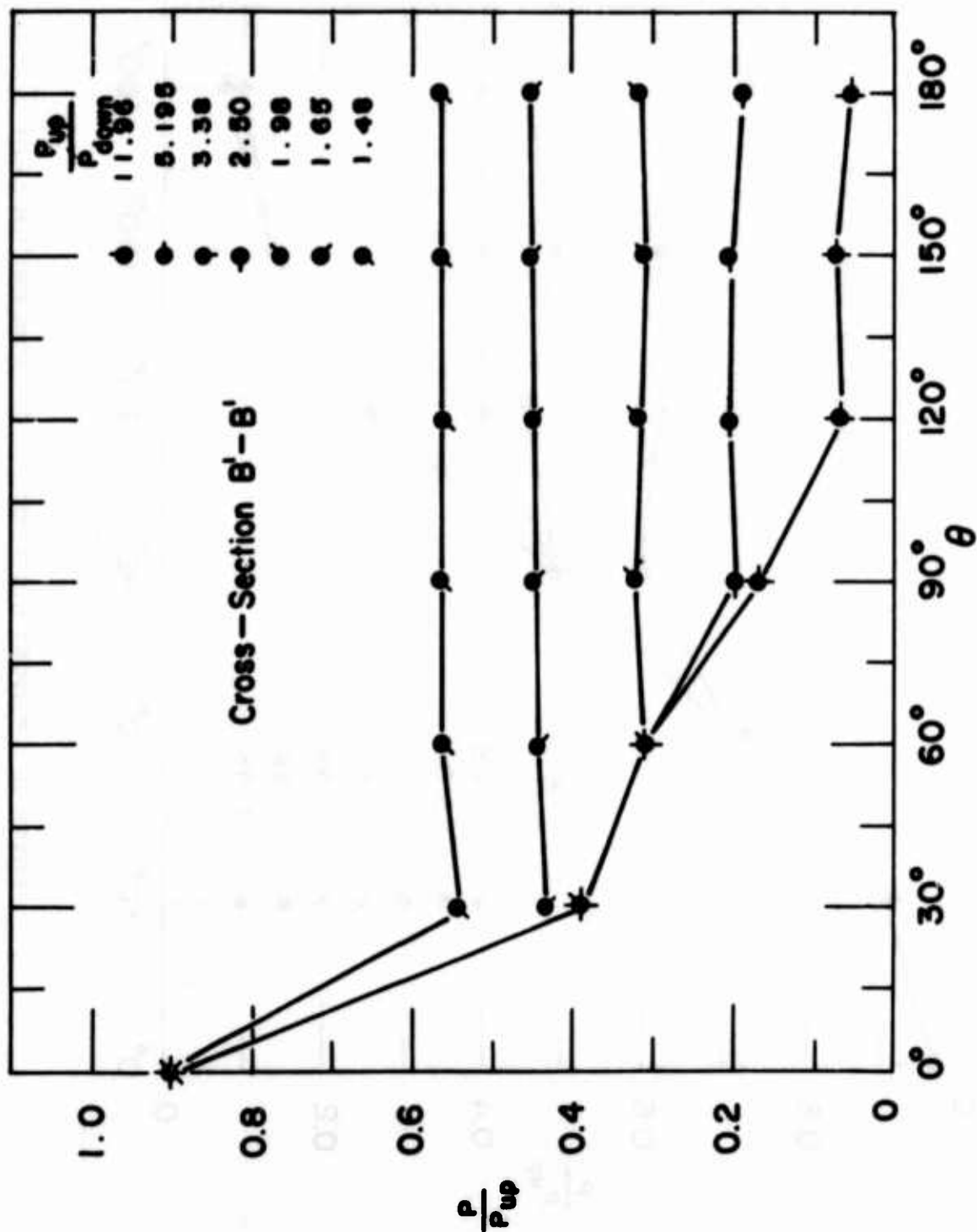


FIGURE 13 PRESSURE DISTRIBUTION FOR CROSS-SECTION B'-B'

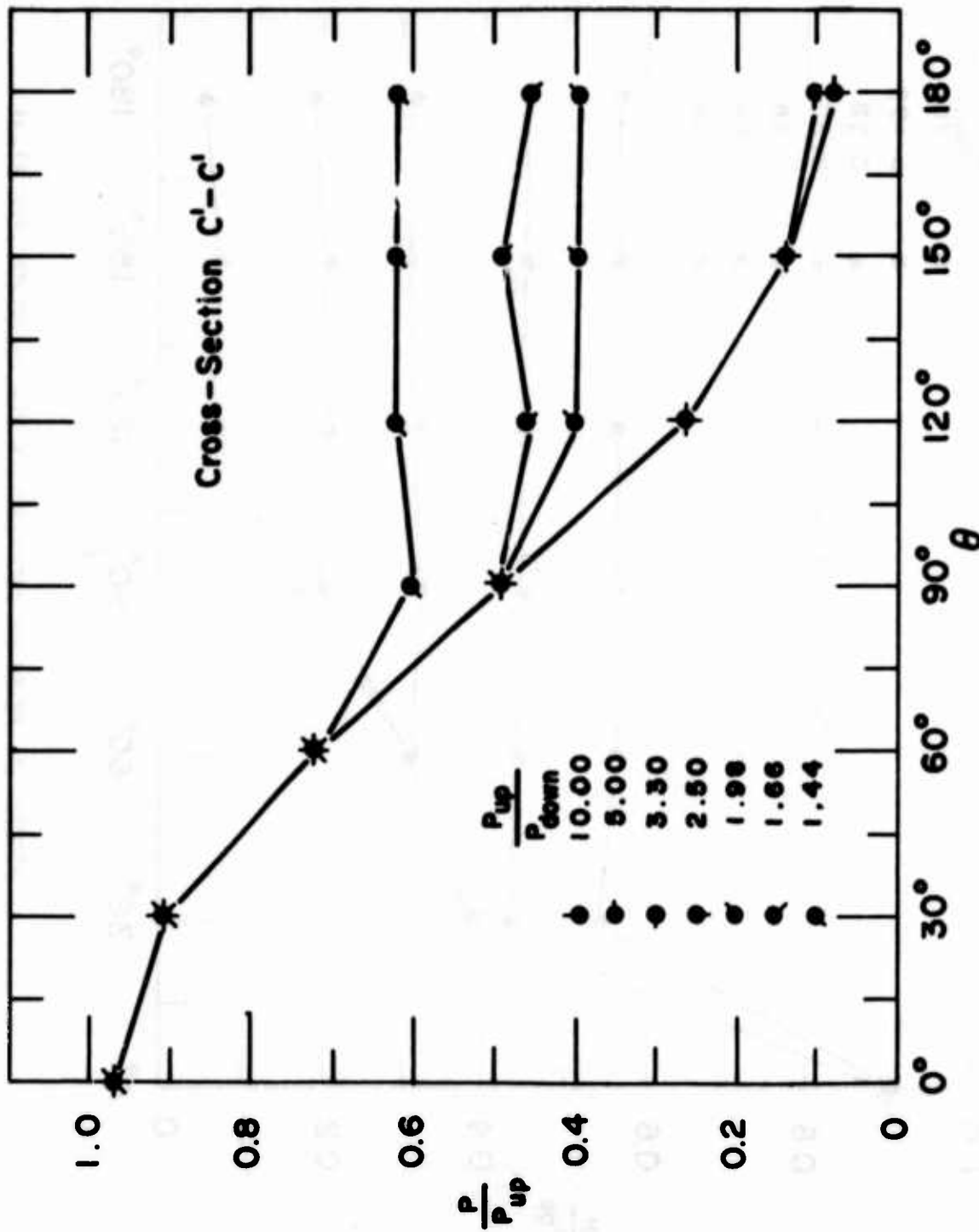


FIGURE 14. PRESSURE DISTRIBUTION FOR CROSS-SECTION C'-C'

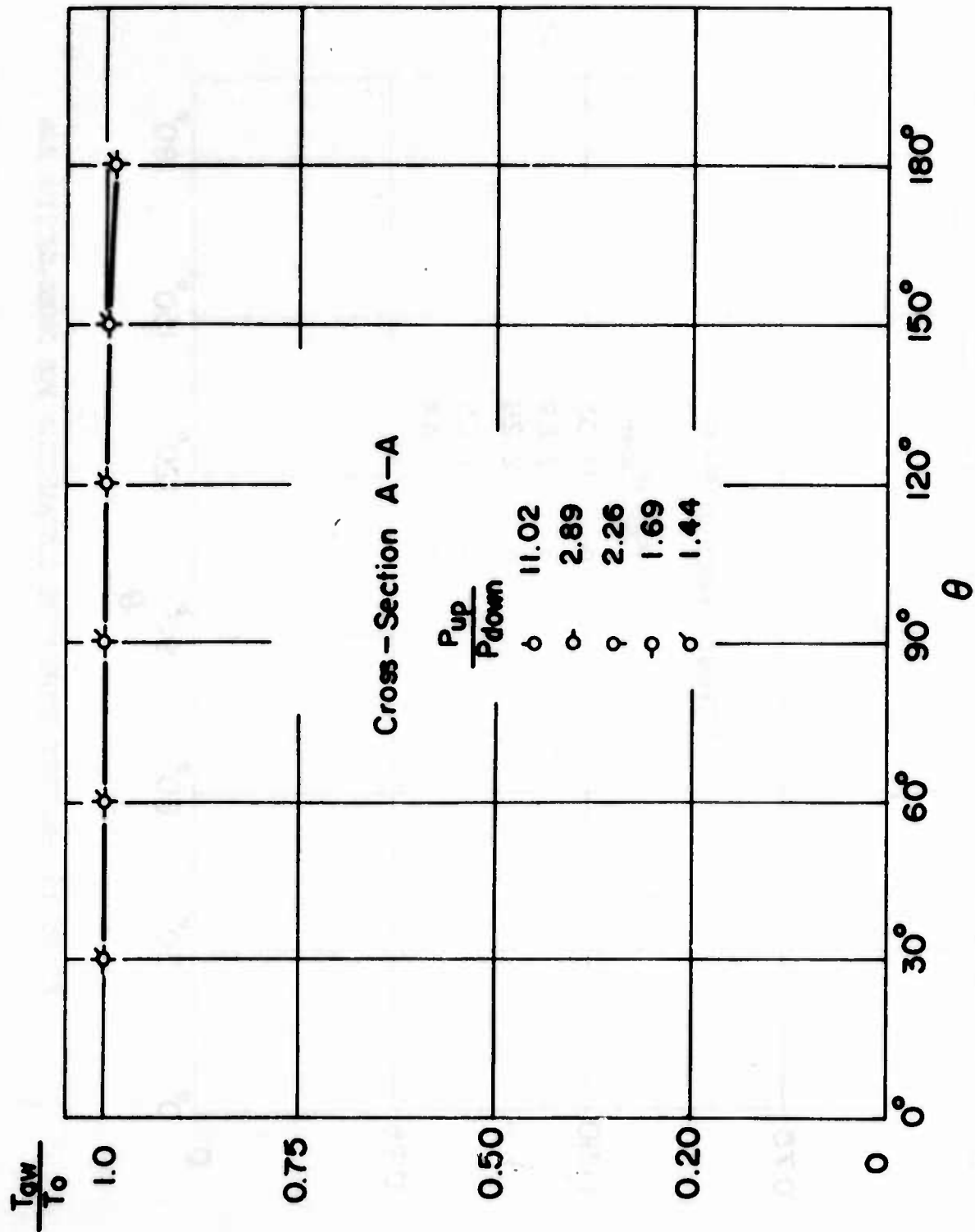


FIGURE 15 RECOVERY TEMPERATURE DISTRIBUTION FOR CROSS-SECTION A-A

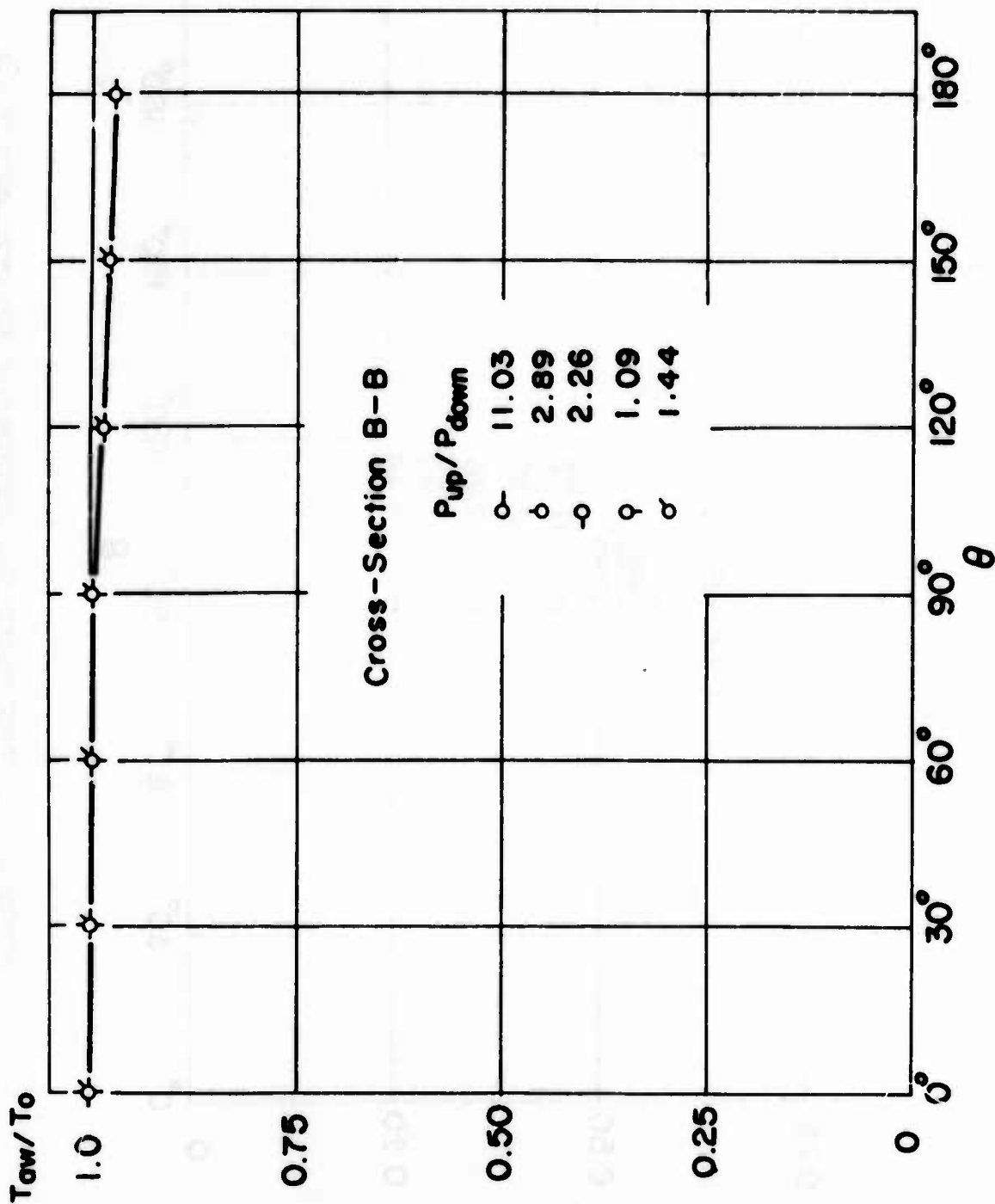


FIGURE 16 RECOVERY TEMPERATURE DISTRIBUTION FOR CROSS-SECTION B-B

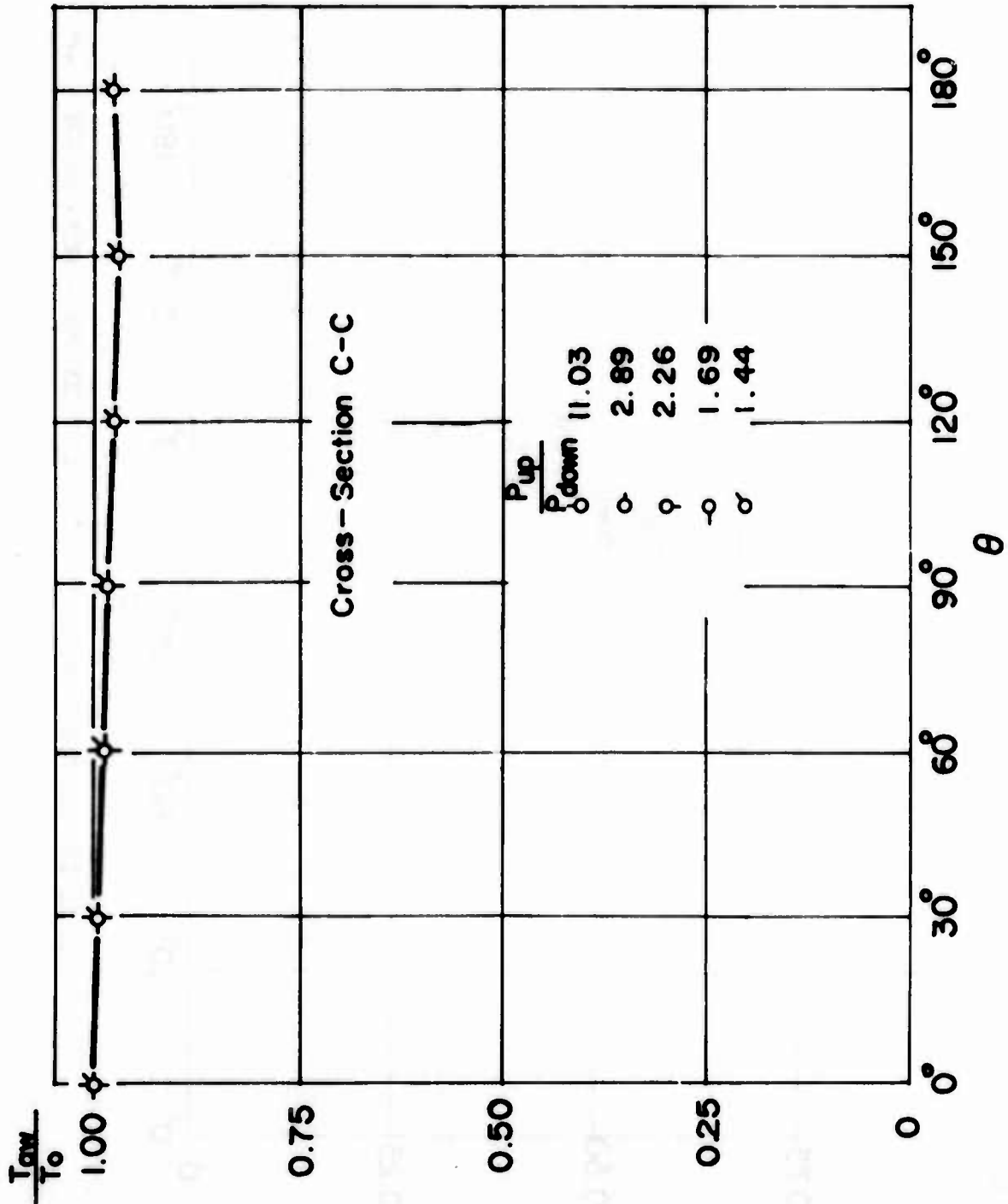


FIGURE 17 RECOVERY TEMPERATURE DISTRIBUTION FOR CROSS-SECTION C-C

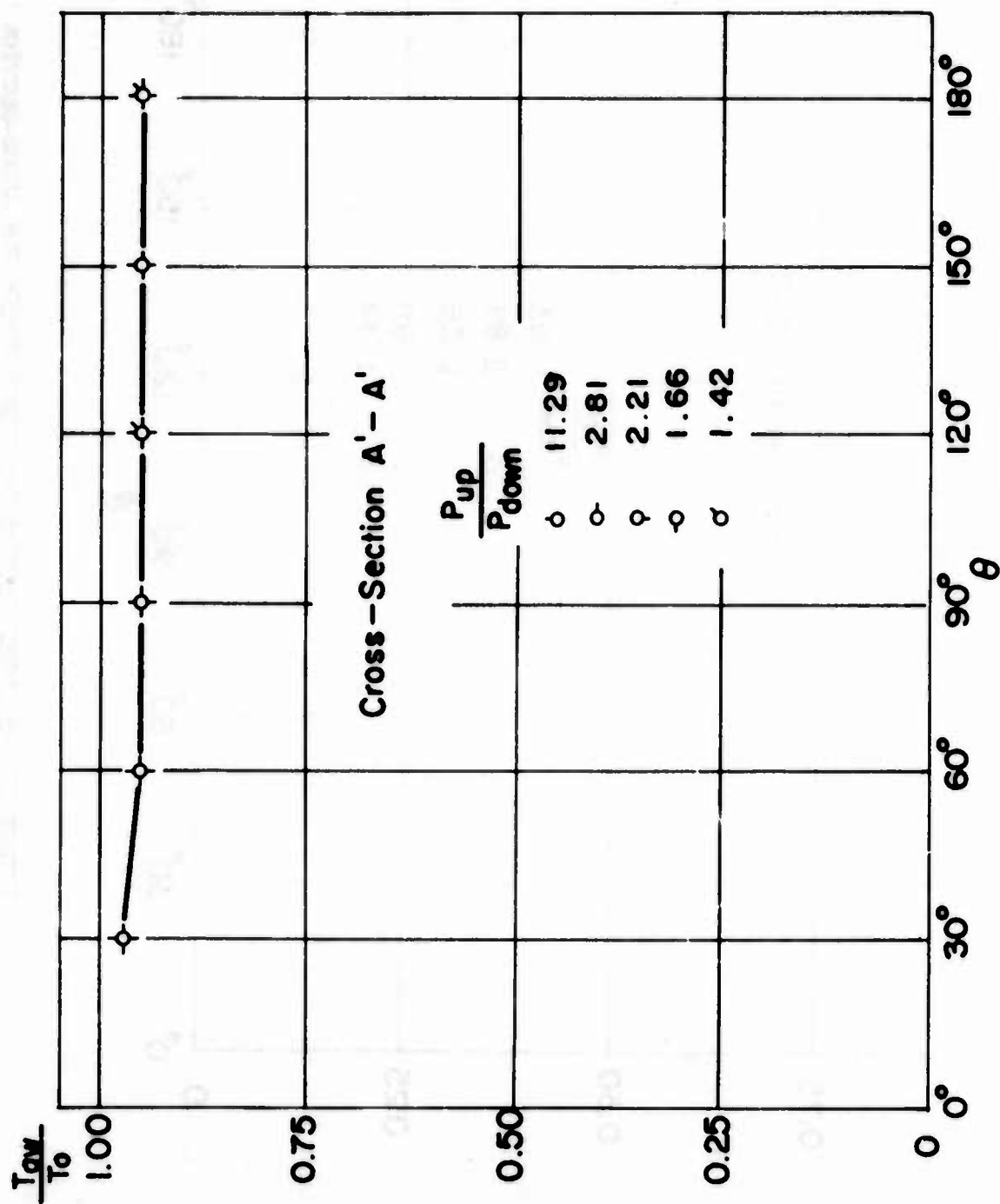


FIGURE 18 RECOVERY TEMPERATURE DISTRIBUTION FOR CROSS-SECTION A' - A'

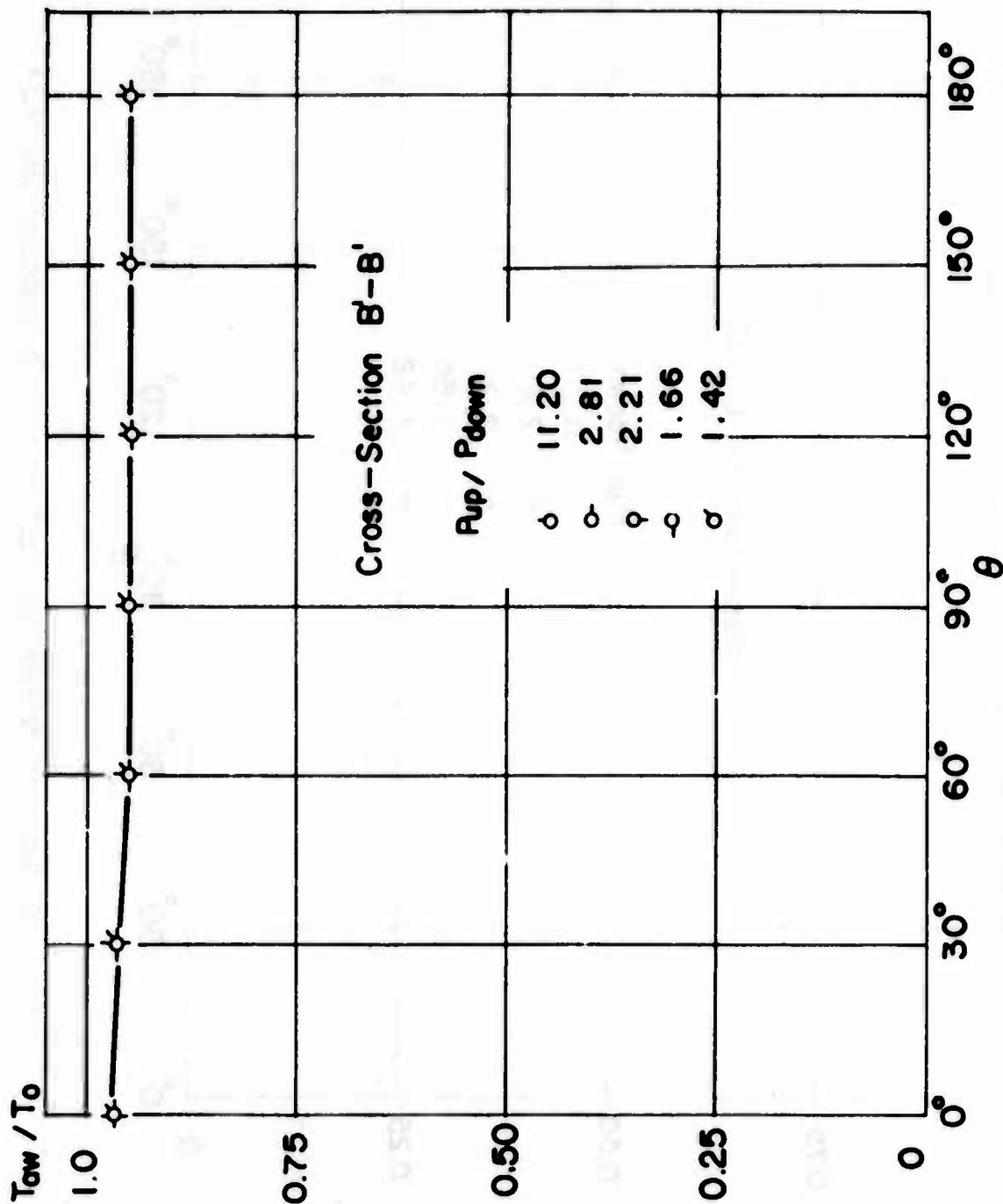


FIGURE 19 RECOVERY TEMPERATURE DISTRIBUTION FOR CROSS-SECTION B'-B'

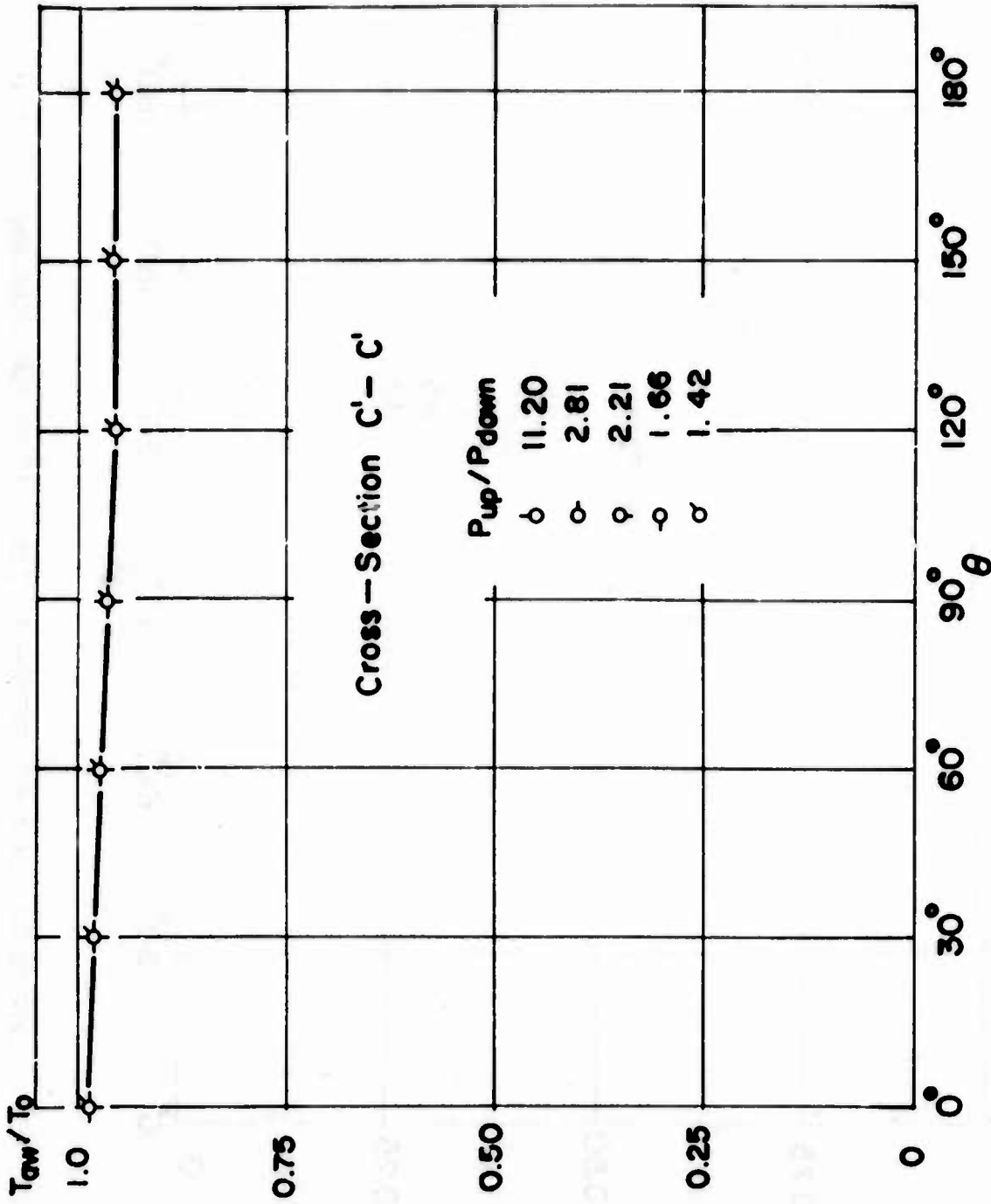


FIGURE 20 RECOVERY TEMPERATURE DISTRIBUTION FOR CROSS-SECTION C'-C'

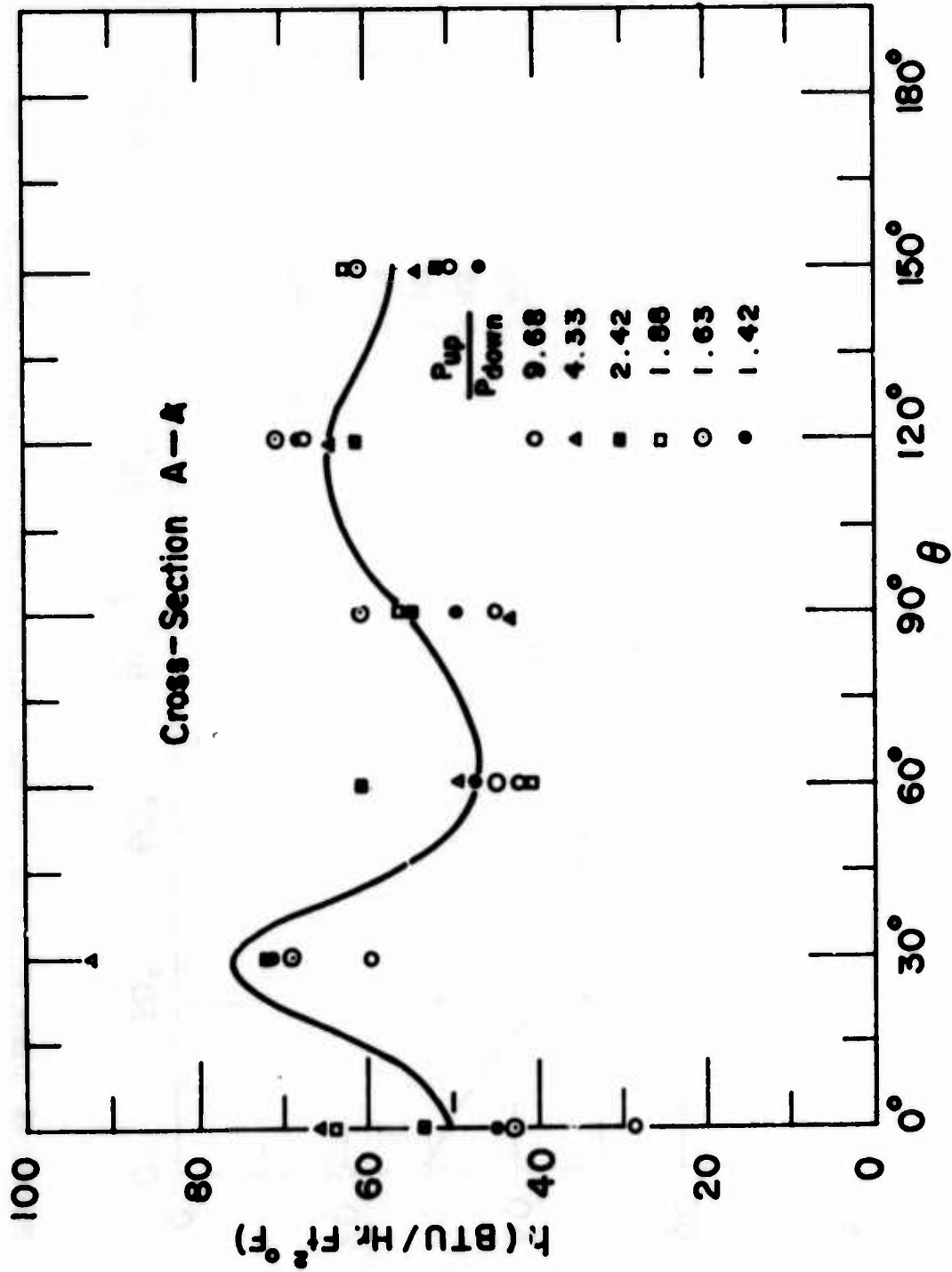


FIGURE 21 DISTRIBUTION OF THE HEAT TRANSFER COEFFICIENTS FOR CROSS-SECTION A-A

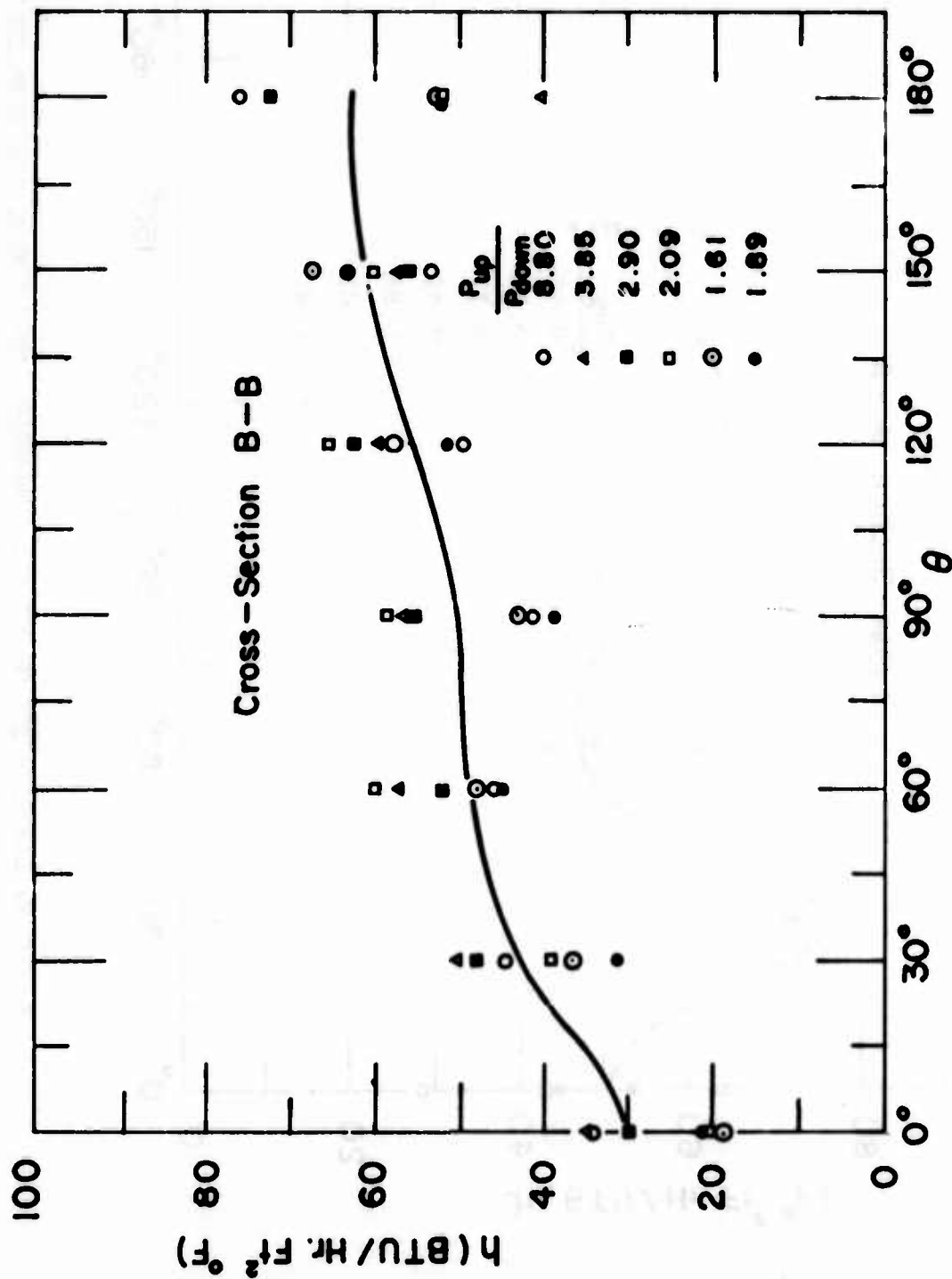


FIGURE 22 DISTRIBUTION OF THE HEAT TRANSFER COEFFICIENTS FOR CROSS-SECTION B-B

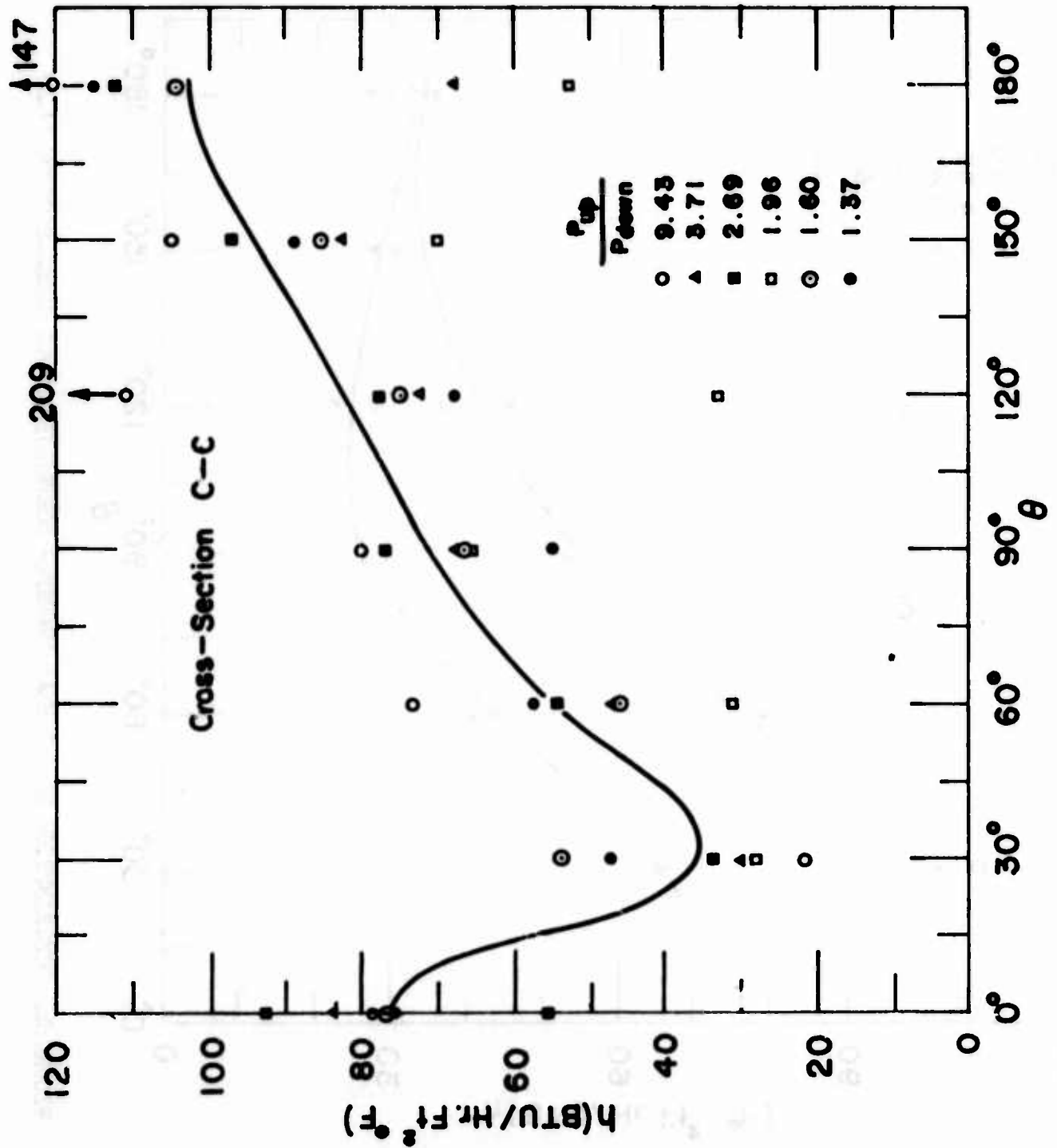


FIGURE 23 DISTRIBUTION OF THE HEAT TRANSFER COEFFICIENTS FOR CROSS-SECTION C-C

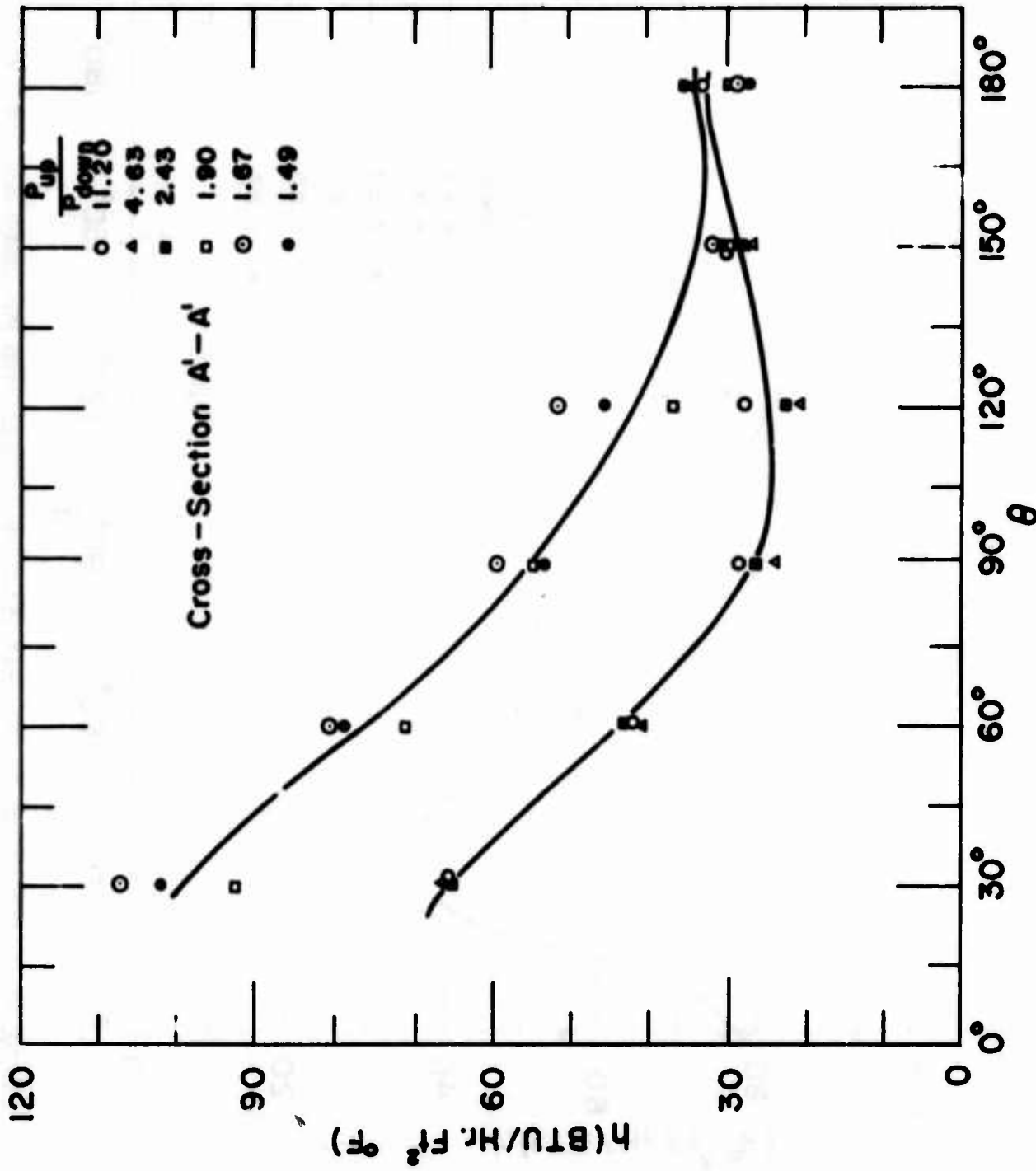


FIGURE 24 DISTRIBUTION OF THE HEAT TRANSFER COEFFICIENTS FOR CROSS-SECTION A'-A'

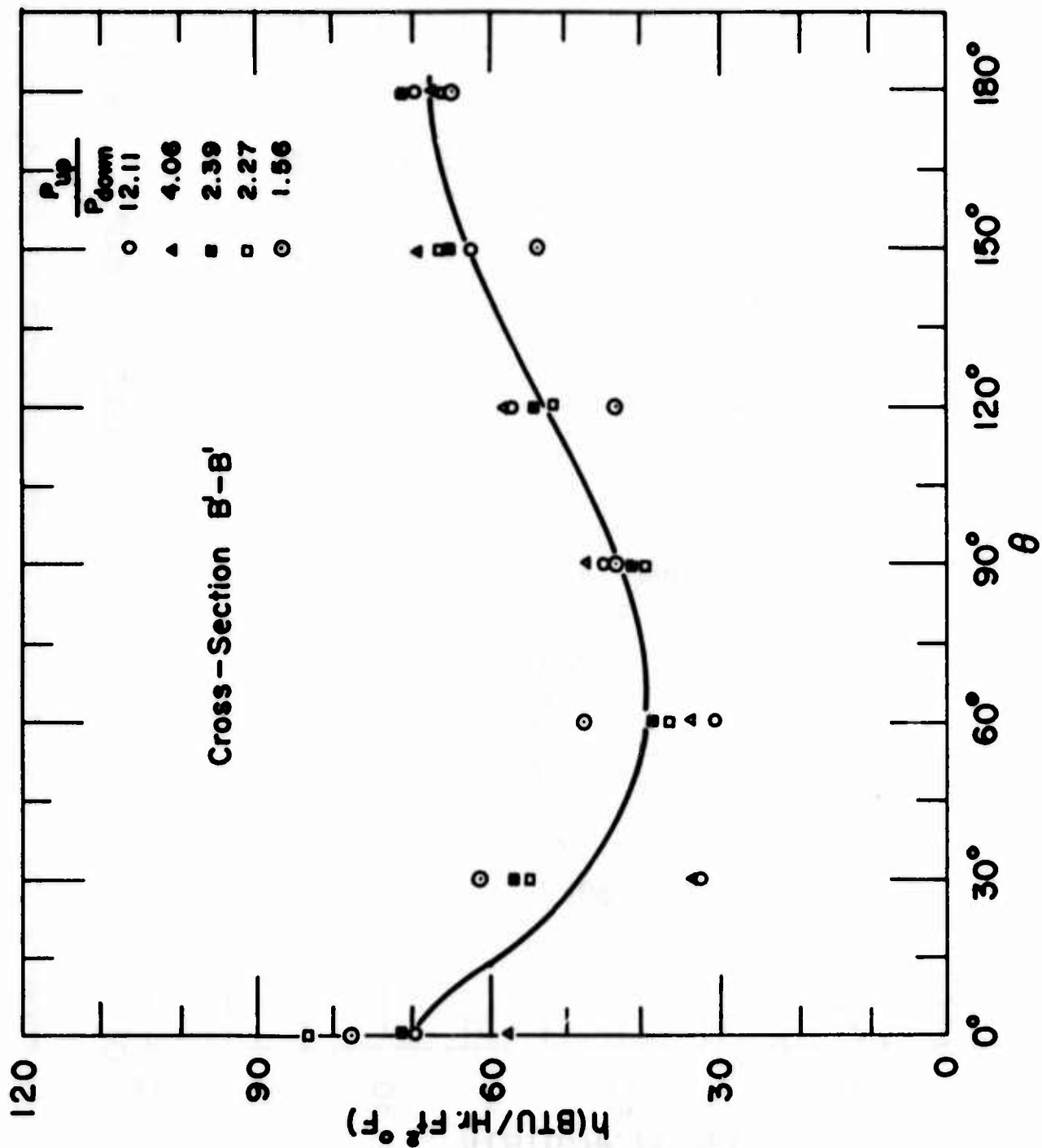


FIGURE 25 DISTRIBUTION OF THE HEAT TRANSFER COEFFICIENTS FOR CROSS-SECTION B'-B'

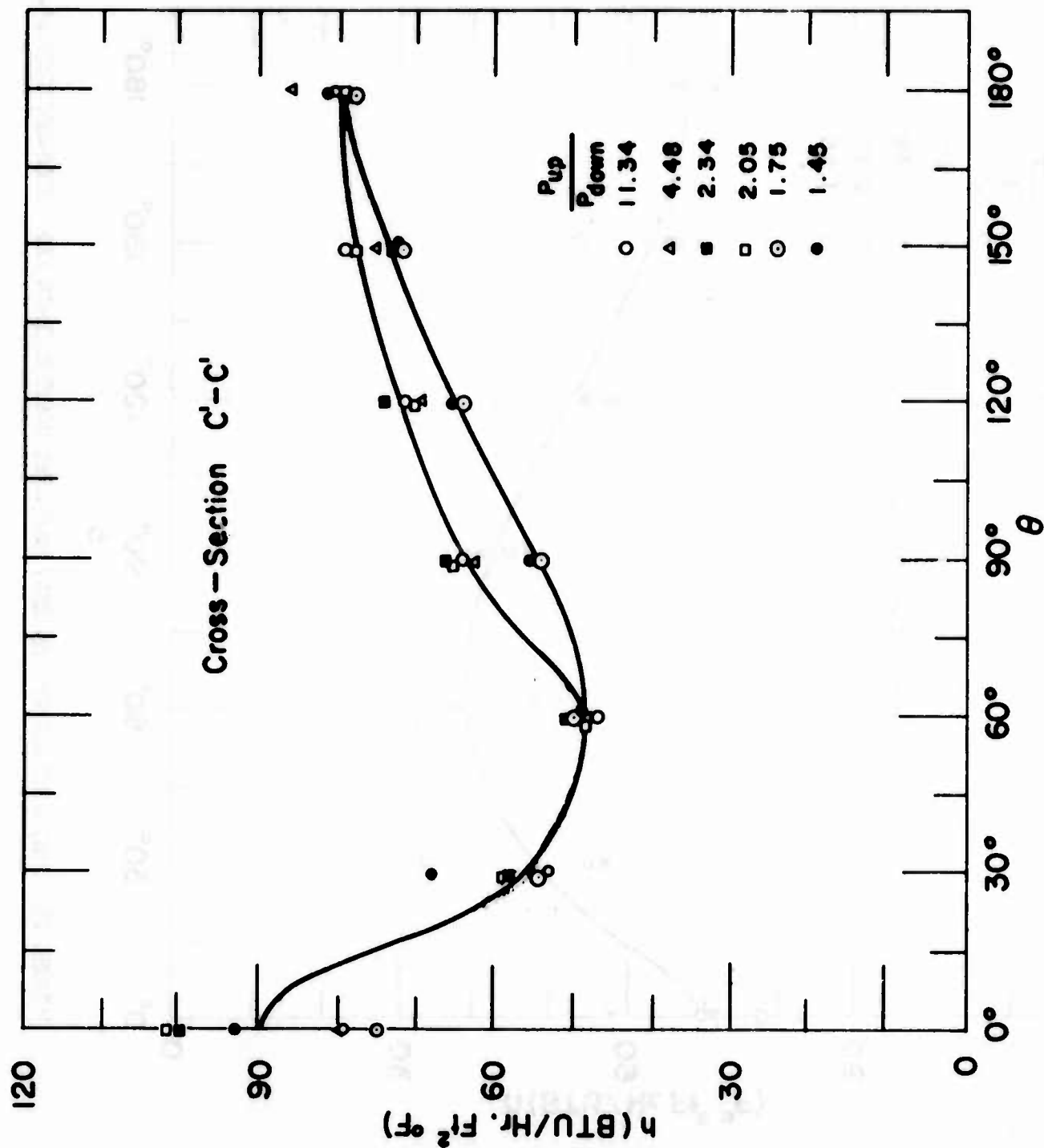


FIGURE 26 DISTRIBUTION OF THE HEAT TRANSFER COEFFICIENTS FOR CROSS-SECTION C'-C'

Cross-Section A-A

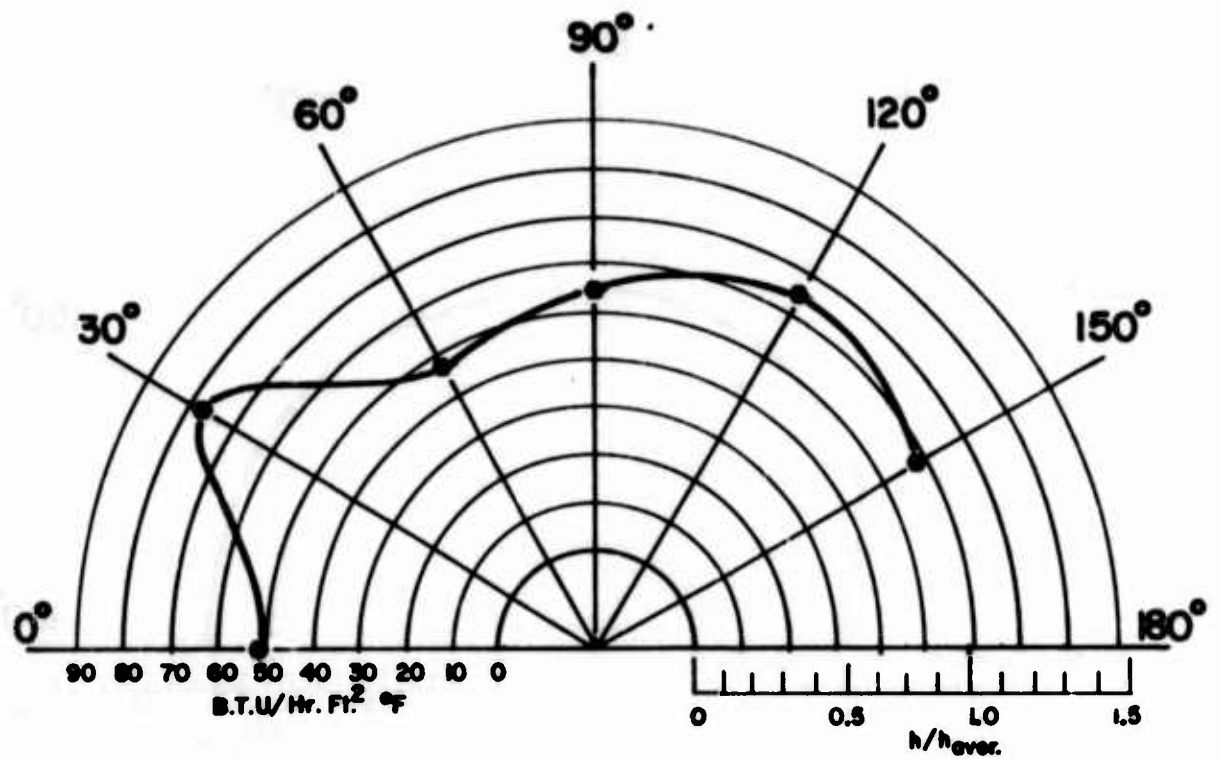


FIGURE 27 DISTRIBUTION OF THE HEAT TRANSFER COEFFICIENTS IN POLAR FORM FOR CROSS-SECTION A-A

Cross-Section B-B

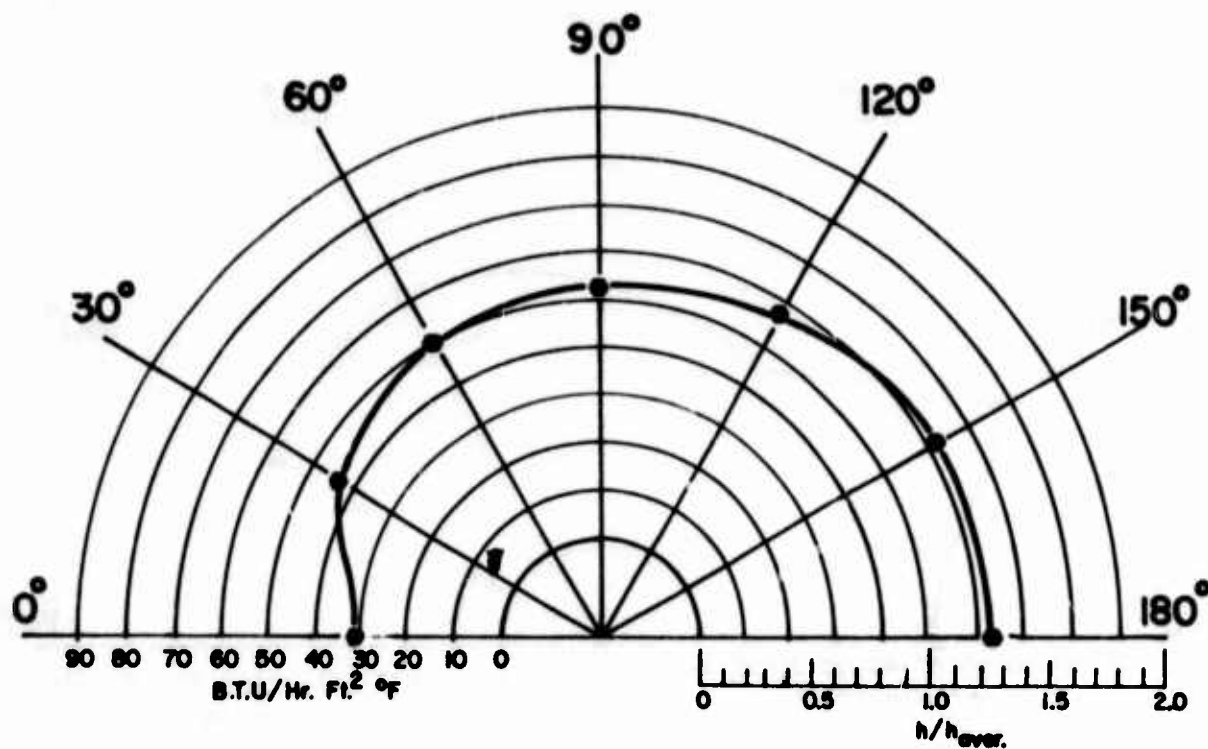


FIGURE 28 DISTRIBUTION OF THE HEAT TRANSFER COEFFICIENTS
IN POLAR FORM FOR CROSS-SECTION B-B

Cross-Section C-C

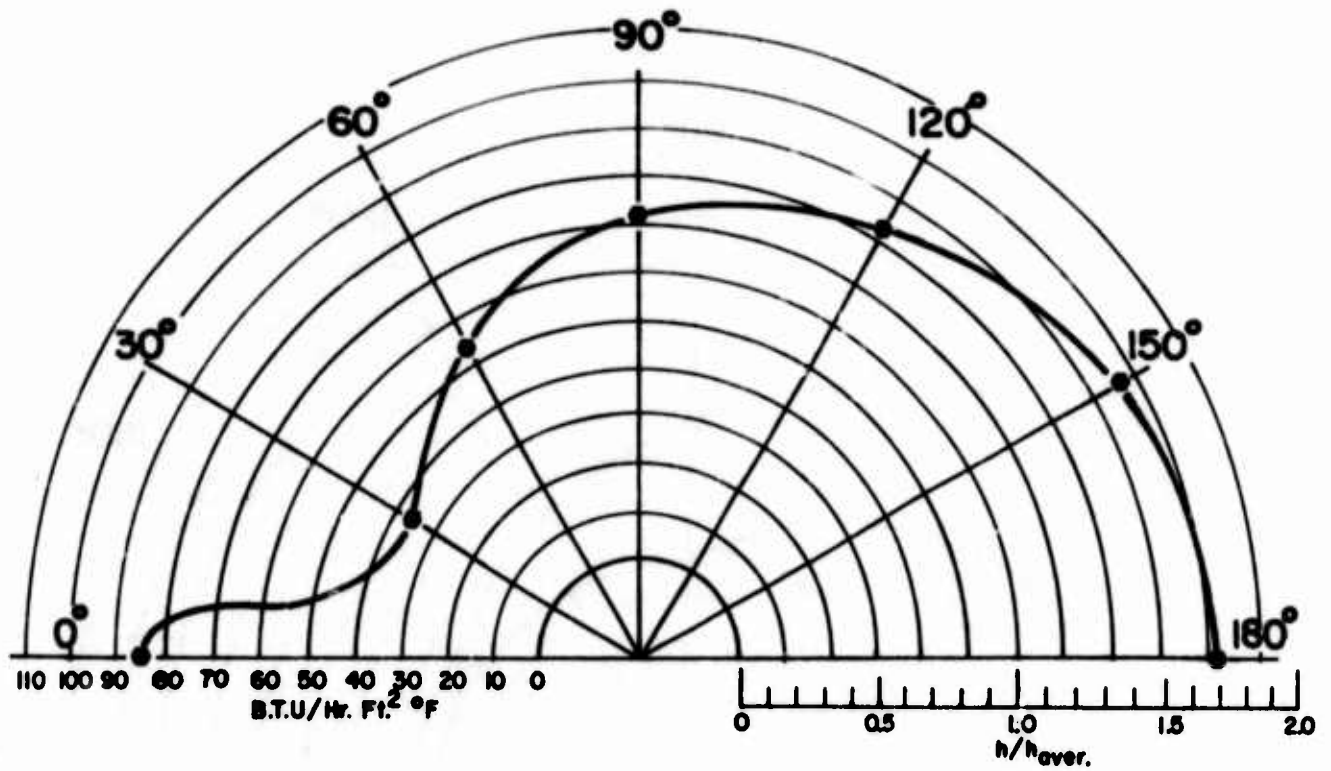
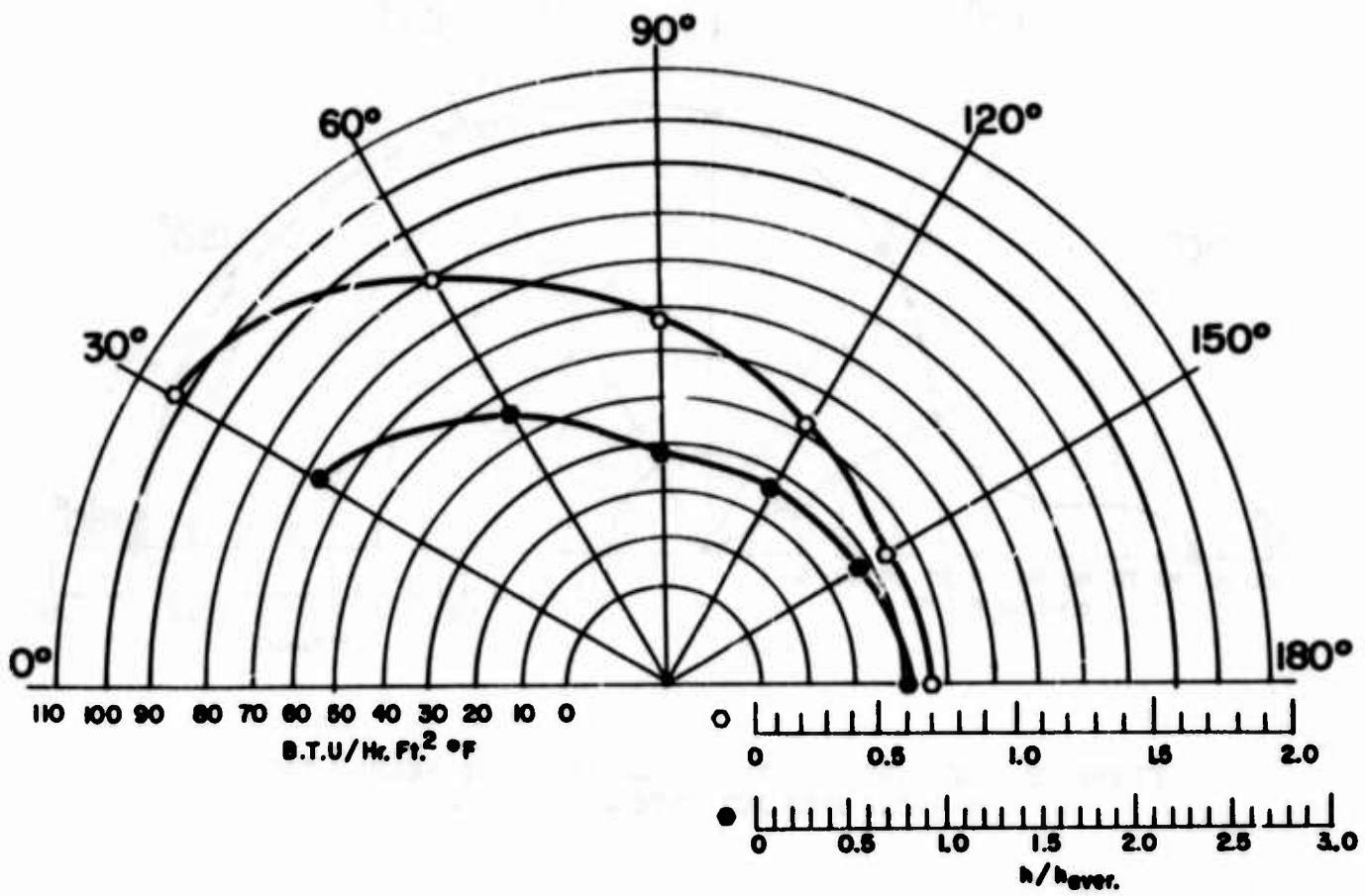


FIGURE 29 DISTRIBUTION OF THE HEAT TRANSFER COEFFICIENTS
IN POLAR FORM FOR CROSS-SECTION C-C

Cross-Section A'-A'



$\frac{P_{up}}{P_{down}}$	○ 1.49	1.67	1.90
	● 2.43	4.63	11.24

FIGURE 30 DISTRIBUTION OF THE HEAT TRANSFER COEFFICIENTS
IN POLAR FORM FOR CROSS-SECTION A'-A'

Cross-Section B'-B'

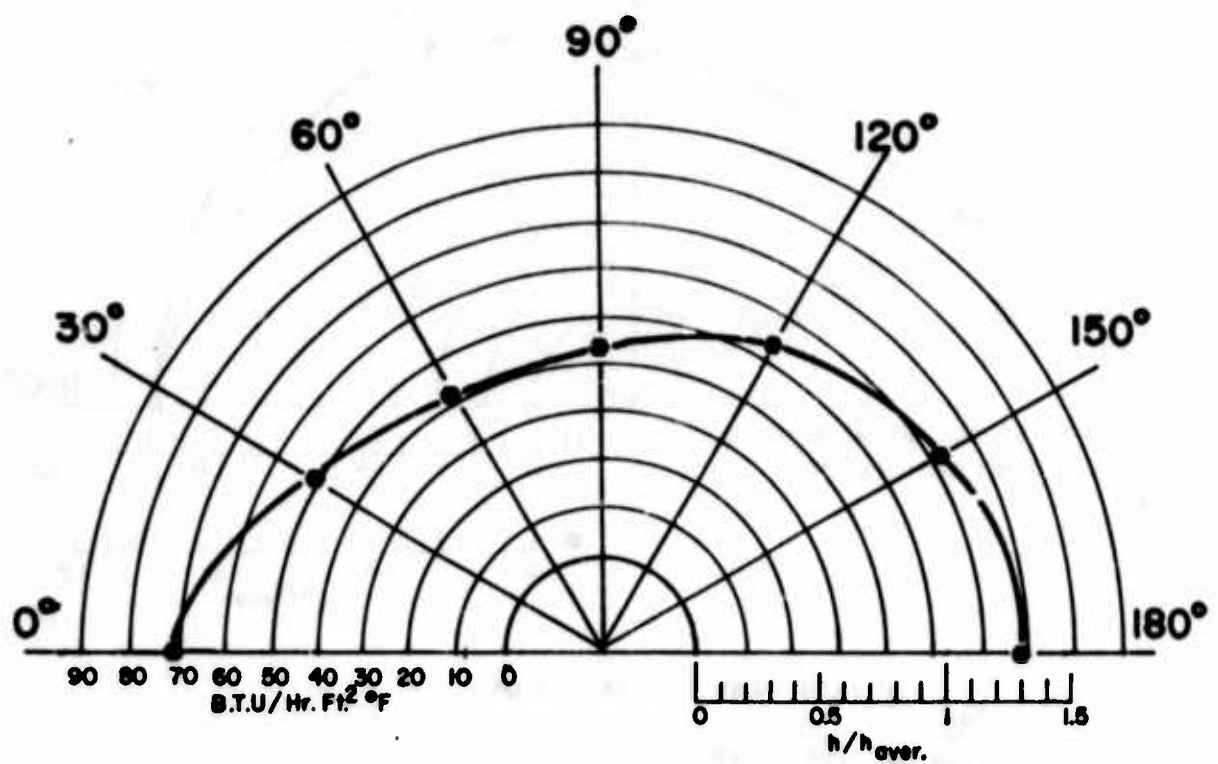
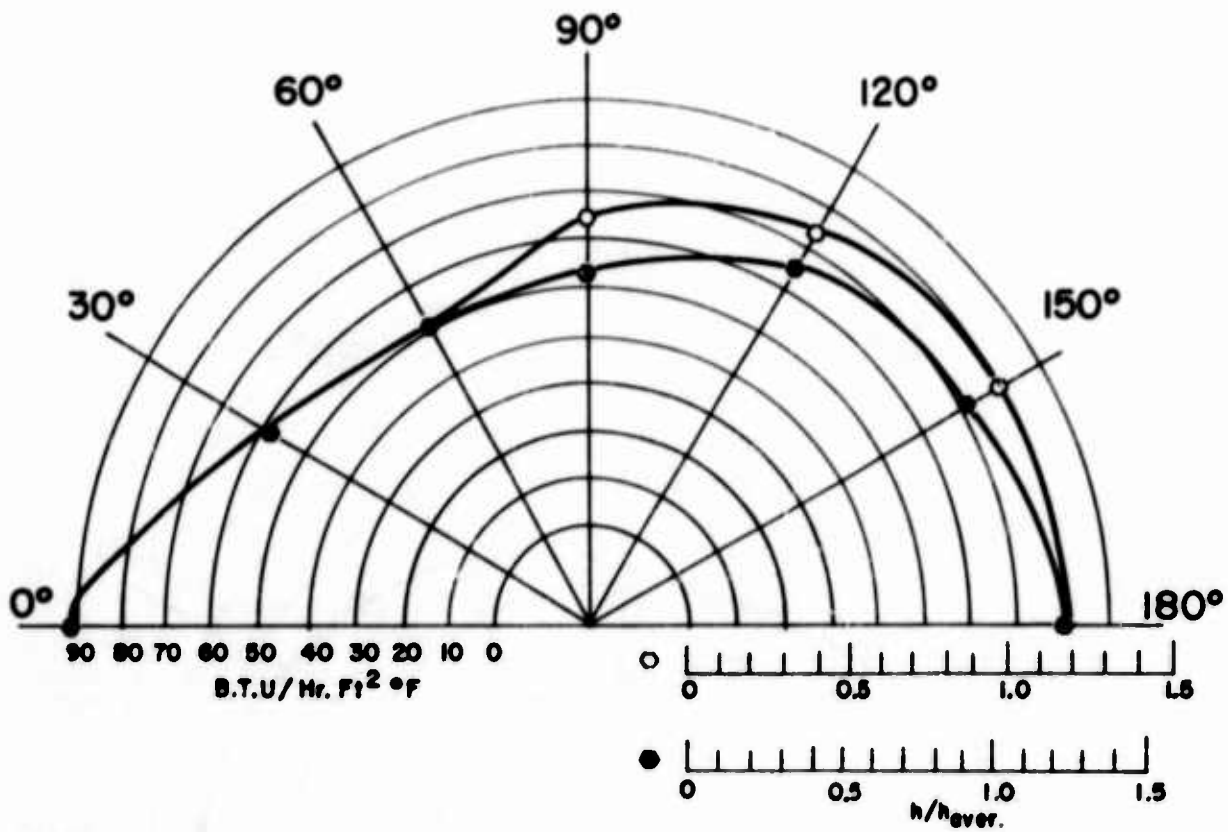


FIGURE 31 DISTRIBUTION OF THE HEAT TRANSFER COEFFICIENTS IN POLAR FORM FOR CROSS-SECTION B'-B'

Cross-Section C'-C'



	○	11.34	4.48	2.34	2.05
$\frac{P_{up}}{P_{down}}$	●	1.75	1.45		

FIGURE 32 DISTRIBUTION OF THE HEAT TRANSFER COEFFICIENTS
IN POLAR FORM FOR CROSS-SECTION C'-C'

APPENDIX

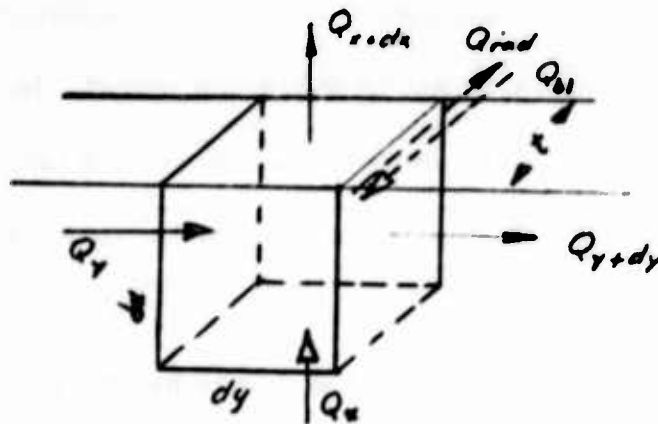
TRANSIENT ENERGY BALANCE

1. Basic Equation

The transient technique relies on the heat capacity of the model skin for the experimental determination of convective heat flux. The general heat balance on a small element of surface must include:

- $q_{b,1}$ - the heat flux from the boundary layer
- q_x - heat conduction in X direction within the skin
- q_y - heat conduction in Y direction within the skin
- q_{rad} - heat loss due to radiation to the wind tunnel (n) and to the model interior (m)

The term $q_{b,1}$, which we wish to determine, should be the dominant term in a good experiment.



The general heat balance equation is written:

$$q_{b,1} dy dx + (q_x - q_{x+dx}) t dy + (q_y - q_{y+dy}) t dx - q_{rad} dx dy = \rho_m dW \frac{dT_w}{dt}$$

where dW is the element of mass lying beneath the surface dA_w .

For a uniform wall thickness, t , and density, ρ_m

$$dW = \rho_m dy dx t$$

Combining all elements of the heat balance and using Taylor's expansion and Fourier's law, the heat balance equation becomes

$$q_{oi} = \rho_m c_{pm} t \frac{dT_w}{dt} - k_m t \left(\frac{\partial^2 T_w}{\partial x^2} + \frac{\partial^2 T_w}{\partial y^2} \right) + \sigma \epsilon_{w-n} (T_w^4 - T_n^4) \quad (1)$$

2. Estimate of Significance of Radiation

It is possible to obtain reasonable, but not precise, estimates of the radiation heat fluxes. Radiation losses to the test section walls and nozzle blocks must be considered; however, radiation exchange into the interior of the model will not be taken in account. In consideration of the extrapolation technique later explained and the uniform temperature distribution of time $t = 0$, the error made under this last assumption is negligible.

In order to estimate the heat exchange by radiation, we assume the model walls are perpendicular to the wind tunnel walls. The heat exchange by radiation in this case will be larger than that corresponding to the actual model. For this case the maximum radiant heat flux for the hypothetical surface was found to be 291 Btu/ft²-hr. Since the smallest

initial temperature potential was 170°F , the radiation heat transfer coefficient $291/170 = 1.71 \text{ Btu/ft}^2 \text{ hr}^{\circ}\text{F}$ was at most 4%, (see Figures 21 through 26) which lies within the error range expected. Based on this calculation, radiation is eliminated from further consideration.

3. Estimate of Significance of Conduction

As was stated before, a uniform temperature distribution along the walls of the bars was necessary in order to eliminate heat-conduction within the skin at the time $\tau = 0$. Because of the influence of the free convection and of the non-symmetry of the model with respect to each point where data has been taken, it was not easy to obtain the desired uniform temperature distribution during the heating process. The largest temperature difference measured at the start of the run within a cross-section was 10°F . On this basis, the largest of the terms $\partial^2 T_w / \partial x^2$ and $\partial^2 T_w / \partial y^2$ in Equation 1 was found to be less than 2.0°F/ft^2 . With this value the conduction term in Equation 1 was less than $0.008 \text{ Btu/ft}^2 \text{ hr}$. Since q_{rad} is of the order of magnitude $10^4 \text{ Btu/ft}^2 \text{ hr}$, the conduction term can be neglected.

4. Experimental Technique

With the help of Equation 1 with the conduction and radiation terms dropped, the experimental technique can be discussed. The model was heated to around 250°F and held until the temperature distribution became uniform. The runs were made during a typical Minnesota summer day during which the tunnel temperature averaged 80°F . Hence the initial temperature

potential was about 170°F. When the model temperatures were stable and uniform, the model was inserted into the wind tunnel. Model temperatures decreased with time as a result of the convective cooling process. Each term in Equation 1 is time dependent. Initially only the storage term and the model nozzle radiation terms contribute. As time proceeds, the other terms increase in importance. The equilibrium situation occurs when the first term on the right reduces to zero, and the model is at the adiabatic wall (T_{aw}) condition.

The accuracy of the method depends to a large extent on the frequency with which reliable thermocouple readings are recorded near the beginning of the run. Hence measurements were taken at only one cross-section at a time, with temperature readings at each point every 1.4 seconds for the cross-sections B-B, C-C, B'-B', C'-C' and every 1.2 seconds for the cross-sections A-A and A'-A'.

Taking data early in a run implies that no surface heat conduction corrections are necessary; a fact which greatly simplifies data reduction. The aerodynamic heat flux is then obtained for the isothermal surface temperature case, which is the most basic and easily specified case and the only case for which most heat transfer analyses apply.

5. Data Reduction

Equation 1 is now written in the form

$$q_{b1} = -h(T_w - T_{aw}) = \rho_m c_{pm} t \frac{dT_w}{dt} \quad (2)$$

For h constant and T_{aw} fixed by the prescribed pressure ratio, integrating Equation 2 yields

$$\frac{T_w - T_{aw}}{T_w(0) - T_{aw}} = e^{-\frac{h \tau}{\rho_m c_m t}} \quad (3)$$

where τ corresponds to the elapsed time from starting when wall temperature was $T_w(0)$. T_{aw} in Equation 3 is computed using the ratio of adiabatic wall temperature to stagnation temperature, defined by

$$r = \frac{T_{aw}}{T_o}$$

This ratio is measured by running for a sufficient length of time (see Section IIIC). Thus the adiabatic wall temperature T_{aw} can be calculated from

$$T_{aw} = r T_o'$$

where T_o' is the stagnation temperature measured for each run. Solving Equation 3 for h

$$h = \frac{\rho_m c_m t}{\tau} \ln_e \left(\frac{T_w - T_{aw}}{T_w(0) - T_{aw}} \right) \quad (4)$$

where T_w corresponds to the temperature at time τ .

Running time was extended for approximately 20-30 seconds after insertion of the grid assembly. This technique allowed a time-temperature

history to be recorded. Then, using this data, the heat transfer coefficient could be computed at any time from Equation 4. However, due to the inherent error in determining the elapsed time from start, two consecutive data points were used. Applying Equation 4 to two different times, τ_1 and τ_2 and reducing we get

$$h = \frac{S_m c_m t}{\tau_2 - \tau_1} \ln_e \left(\frac{T_{w1} - T_{aw}}{T_{w2} - T_{aw}} \right) \quad (5)$$

In Equation 5 the time difference ($\tau_2 - \tau_1$) appears. This was very accurately measured by the Dymec system.

Seven data points were used to calculate heat transfer coefficient values, two points for each h , yielding six different coefficients. These six heat transfer coefficients should be the same if all other modes of heat transfer are absent. However due to conduction, both radially and axially, the coefficients changed with time.

Thus it was decided to plot these calculated coefficients against a dimensionless temperature ratio R_T defined as

$$R_T = \frac{T_{w_{aver}} - T_{aw}}{T_w(0) - T_{aw}}$$

where $T_{w_{aver}}$ is simply a geometric mean of the two successive temperature responses.

Since at the instant of insertion, the heat transfer mode is entirely convection (temperature distribution uniform about periphery),

the most accurate values of h are obtained for small times, i. e., when R_T is near unity.

By plotting the heat transfer coefficient h versus R_T we obtain a history of the convection process. (See Figure 33). The data points were fitted with a least square polynomial with the boundary condition of zero slope for R_T equal to unity. This extrapolation technique then afforded a heat transfer coefficient independent of any conduction effects.

This method of analysis proved adequate for the majority of runs. However, for some runs where the initial point was inconsistent, the time temperature histories were graphically plotted and Equation 2 was applied directly. (See Figure 34).

The extrapolated values or hand plotted ones are then the heat transfer coefficients used throughout this report.

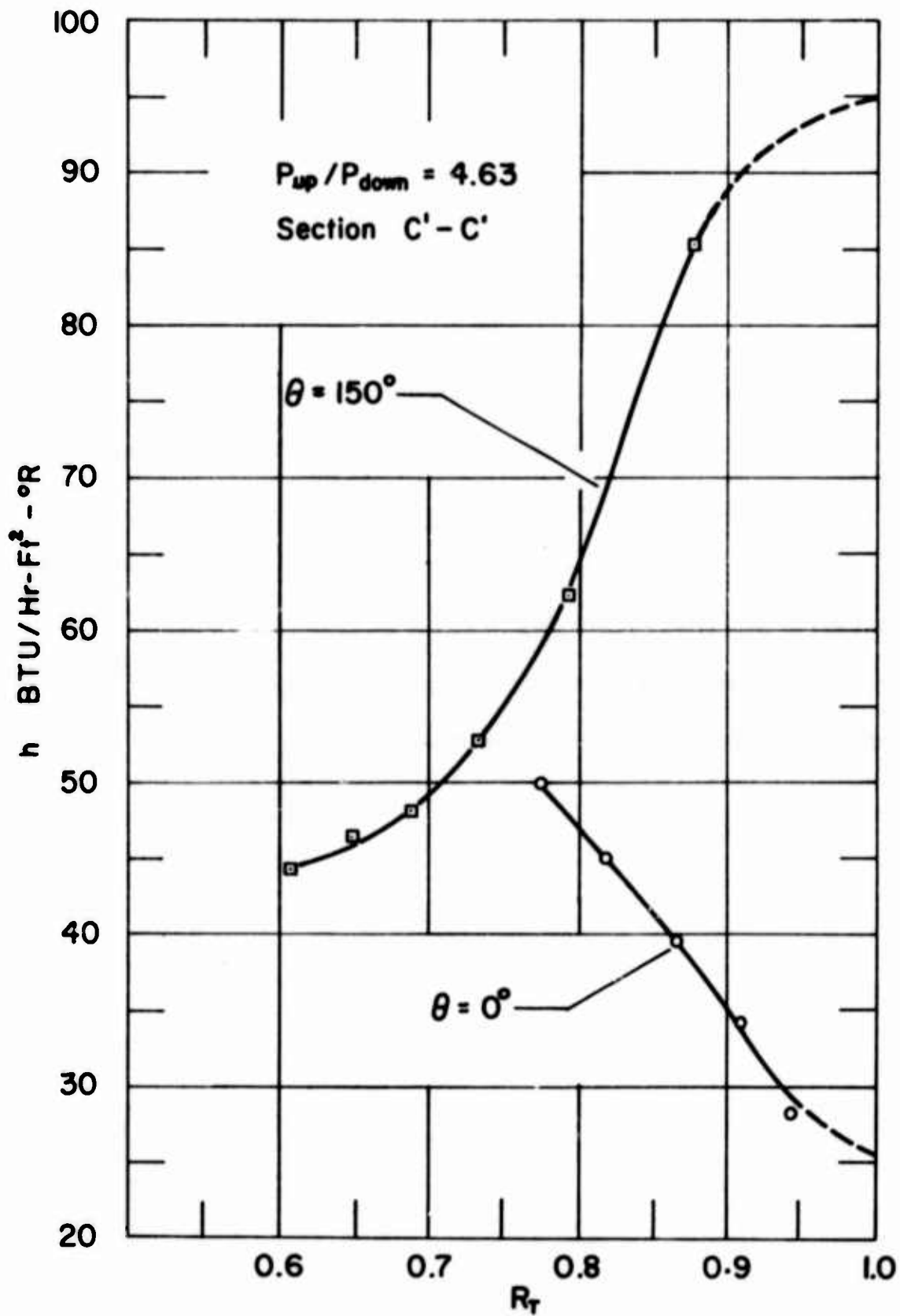


FIGURE 33 TYPICAL EXTRAPOLATION TECHNIQUE FOR HEAT TRANSFER COEFFICIENT

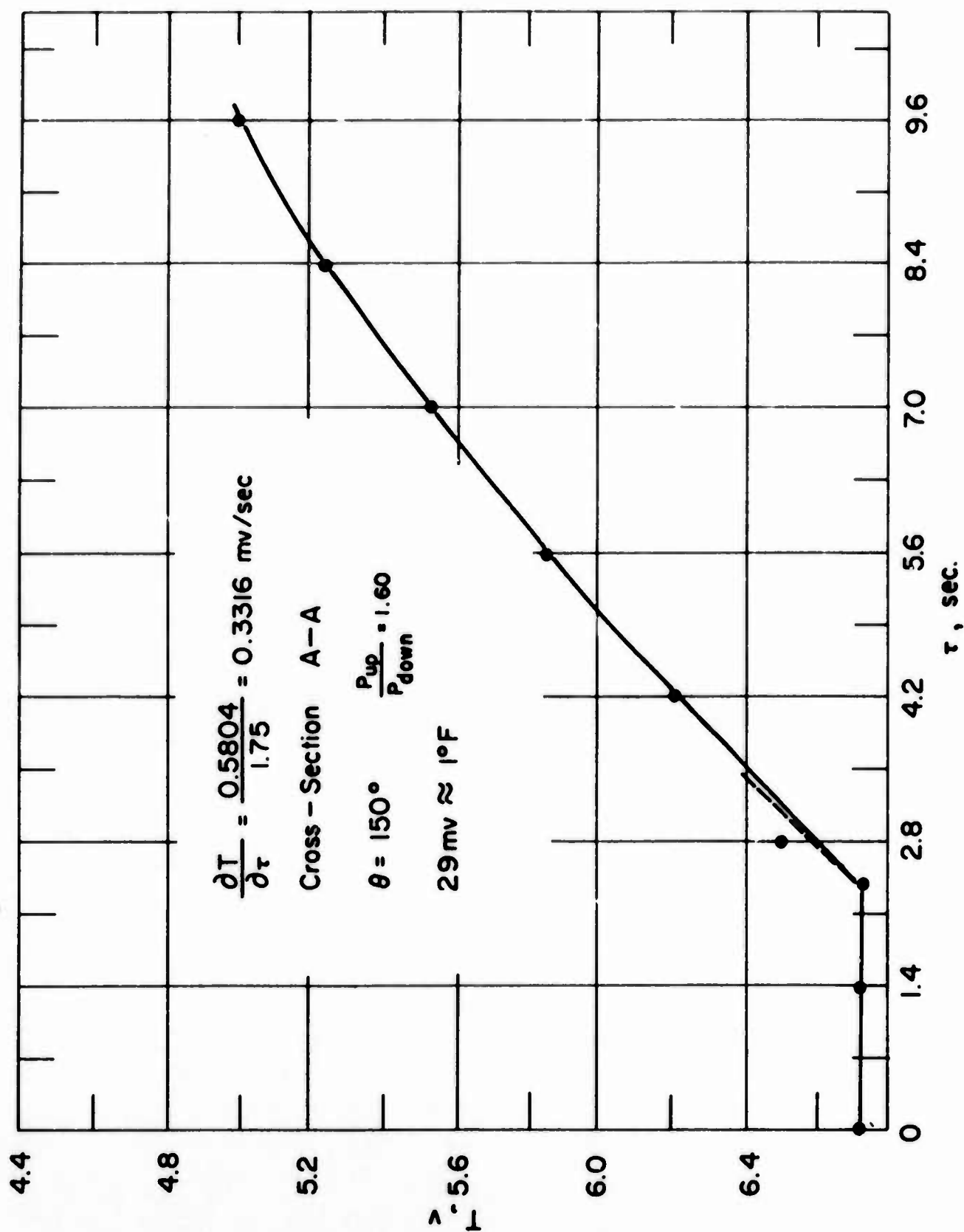


FIGURE 34 TYPICAL TEMPERATURE-TIME HISTORY

Unclassified

Security Classification

DOCUMENT CONTROL DATA - R&D		
(Security classification of title, body of abstract and indexing annotation must be entered when the overall report is classified)		
1. ORIGINATING ACTIVITY (Corporate author) University of Minnesota Institute of Technology Mechanical Engineering Dept. Minneapolis, Minn. 55455		2a. REPORT SECURITY CLASSIFICATION Unclassified
		2b. GROUP n/a
3. REPORT TITLE An Experimental Study of the Distribution of Convective Heat Transfer to a Large-Scale Model of Parachute Cloth		
4. DESCRIPTIVE NOTES (Type of report and inclusive dates) Final Report December 1964 - December 1965		
5. AUTHOR(S) (Last name, first name, initial) Eckert, E. R. G. et al		
6. REPORT DATE May 1966	7a. TOTAL NO. OF PAGES 57	7b. NO. OF REFS 2
8a. CONTRACT OR GRANT NO. AF33(657)-11688	8b. ORIGINATOR'S REPORT NUMBER(S) AFFDL-TR-66-13	
a. PROJECT NO. 6065 c. Task No. 606505 d.	8b. OTHER REPORT NO(S) (Any other numbers that may be assigned this report)	
10. AVAILABILITY/LIMITATION NOTICES Qualified requesters may obtain copies of this report from DDC. This document is subject to special export controls and each transmittal to foreign governments or foreign nationals may be made only with prior approval of the AF Flight Dynamics Laboratory.		
11. SUPPLEMENTARY NOTES n/a	12. SPONSORING MILITARY ACTIVITY AFFDL (FDFR) WPAFB, Ohio	
13. ABSTRACT Experiments on pressure distribution and heat transfer on a grid simulating a parachute cloth were performed. The porosity of the grid was 25%. A pressurized wind-tunnel served as the flow facility. The average approach of the flow was 134 feet per second. The pressure ratio P_{up}/P_{down} was considered as the main variable and varied from around 11 to 1.45. A transient energy balance was used to calculate local heat transfer.		

DD FORM 1473
1 JAN 64

Unclassified

Security Classification

Unclassified

Security Classification

14 KEY WORDS	LINK A		LINK B		LINK C	
	ROLE	WT	ROLE	WT	ROLE	WT
Heat Transfer Supersonic Parachutes Wind Tunnel Investigations Pressure Distribution Aerodynamic Heating						

INSTRUCTIONS

1. ORIGINATING ACTIVITY: Enter the name and address of the contractor, subcontractor, grantee, Department of Defense activity or other organization (*corporate author*) issuing the report.

2a. REPORT SECURITY CLASSIFICATION: Enter the overall security classification of the report. Indicate whether "Restricted Data" is included. Marking is to be in accordance with appropriate security regulations.

2b. GROUP: Automatic downgrading is specified in DoD Directive 5200.10 and Armed Forces Industrial Manual. Enter the group number. Also, when applicable, show that optional markings have been used for Group 3 and Group 4 as authorized.

3. REPORT TITLE: Enter the complete report title in all capital letters. Titles in all cases should be unclassified. If a meaningful title cannot be selected without classification, show title classification in all capitals in parentheses immediately following the title.

4. DESCRIPTIVE NOTES: If appropriate, enter the type of report, e.g., interim, progress, summary, annual, or final. Give the inclusive dates when a specific reporting period is covered.

5. AUTHOR(S): Enter the name(s) of author(s) as shown on or in the report. Enter last name, first name, middle initial. If military, show rank and branch of service. The name of the principal author is an absolute minimum requirement.

6. REPORT DATE: Enter the date of the report as day, month, year, or month, year. If more than one date appears on the report, use date of publication.

7a. TOTAL NUMBER OF PAGES: The total page count should follow normal pagination procedures, i.e., enter the number of pages containing information.

7b. NUMBER OF REFERENCES: Enter the total number of references cited in the report.

8a. CONTRACT OR GRANT NUMBER: If appropriate, enter the applicable number of the contract or grant under which the report was written.

8b, 8c, & 8d. PROJECT NUMBER: Enter the appropriate military department identification, such as project number, subproject number, system numbers, task number, etc.

9a. ORIGINATOR'S REPORT NUMBER(S): Enter the official report number by which the document will be identified and controlled by the originating activity. This number must be unique to this report.

9b. OTHER REPORT NUMBER(S): If the report has been assigned any other report numbers (*either by the originator or by the sponsor*), also enter this number(s).

10. AVAILABILITY/LIMITATION NOTICES: Enter any limitations on further dissemination of the report, other than those imposed by security classification, using standard statements such as:

- "Qualified requesters may obtain copies of this report from DDC."
- "Foreign announcement and dissemination of this report by DDC is not authorized."
- "U. S. Government agencies may obtain copies of this report directly from DDC. Other qualified DDC users shall request through _____."
- "U. S. military agencies may obtain copies of this report directly from DDC. Other qualified users shall request through _____."
- "All distribution of this report is controlled. Qualified DDC users shall request through _____."

If the report has been furnished to the Office of Technical Services, Department of Commerce, for sale to the public, indicate this fact and enter the price, if known.

11. SUPPLEMENTARY NOTES: Use for additional explanatory notes.

12. SPONSORING MILITARY ACTIVITY: Enter the name of the departmental project office or laboratory sponsoring (*paying for*) the research and development. Include address.

13. ABSTRACT: Enter an abstract giving a brief and factual summary of the document indicative of the report, even though it may also appear elsewhere in the body of the technical report. If additional space is required, a continuation sheet shall be attached.

It is highly desirable that the abstract of classified reports be unclassified. Each paragraph of the abstract shall end with an indication of the military security classification of the information in the paragraph, represented as (TS), (S), (C), or (U).

There is no limitation on the length of the abstract. However, the suggested length is from 150 to 225 words.

14. KEY WORDS: Key words are technically meaningful terms or short phrases that characterize a report and may be used as index entries for cataloging the report. Key words must be selected so that no security classification is required. Identifiers, such as equipment model designation, trade name, military project code name, geographic location, may be used as key words but will be followed by an indication of technical context. The assignment of links, rules, and weights is optional.

Unclassified

Security Classification